Treatment of Wastewater Containing Pharmaceutical Micropollutants by Adsorption under Flow in Highly Porous Carbon Monoliths

Wassim Sebai, Sher Ahmad, Nicolas Brun, Thomas Cacciaguerra, Didier Cot, Alexis Boccheciampe, Perrine Chaurand, Clement Levard, M-P. Belleville, José Sanchez-Marcano, et al.

Treatment of wastewater containing pharmaceutical micropollutants by adsorption under flow in highly porous carbon monoliths

Wassim Sebai[1, 2], Sher Ahmad[2], Nicolas Brun[1], Thomas Cacciaguerra[1], Didier Cot[2], Alexis Boccheciampe[3], Perrine Chaurand[3], Clement Levard[3], Marie-Pierre Belleville[2], Jose Sanchez-Marcano[2], Anne Galarneau[1*]

[1]ICGM, Univ Montpellier, CNRS, ENSCM, 34293 Montpellier, France.

[2]IEM, Univ Montpellier, CNRS, ENSCM, 34095 Montpellier, France.

[3]Aix Marseille Univ, CNRS, IRD, INRAE, Coll France, CEREGE, 13090 Aix en Provence, France

*corresponding author: anne.galarneau@enscm.fr

Abstract

Flow-through reactors made of highly porous hierarchical micro-/meso-/macroporous carbon monoliths (CM) were developed to decontaminate water-containing pharmaceutical micropollutants (antibiotics). CM were prepared from hierarchical meso-/macroporous silica monoliths as sacrificial templates after impregnation with sucrose as carbon precursor, hydrothermal carbonization, and subsequent pyrolysis and dissolution of silica by NaOH. CM were fully characterized by nitrogen sorption at 77 K, Hg porosimetry, SEM, TEM, microtomography, permeability measurements, XPS, chemical analysis. CM exhibits high surface area (1058 $m^2\ g^{-1}$), high pore volume (6.5 mL g^{-1}), high permeability, homogeneous interconnected macropores network (22 μm), bimodal mesopores (6, 15 nm), micropores (0.85 nm), high amount of C=O and COO^- groups. There are basic in water (pH 9) and negatively charged. First, adsorption of a single pharmaceutical molecule, tetracycline (TC), was studied. Isotherms of adsorption, kinetics and diffusion were used to study the adsorption mechanism on CM and the process was found to be governed by electrostatic interactions. Then, a mixture of several antibiotics (ciprofloxacin, amoxicillin, sulfamethoxazole, TC, 20 mg L^{-1} each) was used. Sorption capacity for antibiotics was as high as 815 mg g^{-1}. In a recirculation flow configuration, with a flow rate of 1 mL min^{-1}, CM was able to remove 93% of the antibiotics. These CM could represent a highly efficient solution for the purification of real wastewater containing pharmaceutical molecules, which are generally found at much lower concentrations

(from a few ng L^{-1} to µg L^{-1}). Regeneration of CM was successfully carried out by washing with HCl (0.1 M).

1. Introduction

Many molecules like drug residues, pesticides or chemical compounds, which are used in medical therapy, cosmetics and food products, are considered as refractory micro-pollutants (MP) because they are still present at the exit of wastewaters treatment plants (WWTP). MP were first identified in treated wastewaters in the United States and Europe between the 1960's and 1970's.[1-2] This issue subsequently generated considerable interest in the scientific community after a correlation was established between the presence of these MP and the feminization of fish living near disposal of treated wastewaters, due to their endocrine-disrupting effect.[3] Later, many other negative effects of the presence of these substances in waters have been observed in wildlife. For example, the presence of diclofenac, a nonsteroidal anti-inflammatory drug, has been directly correlated with kidney failure in vultures, contributing to a decline in their population in the Indian subcontinent by more than 95% since the 1990s.[4] Scientists are gaining a better understanding of the health effects of MP. Some are able to attach to receptors present in or on human and animal cells, instead of endogenous molecules. These compounds are considered as "endocrine disruptors" and may pose a risk if they lead to the disruption of certain physiological mechanisms. The toxicity of several MP has already been studied, e.g., for bisphenol A, whose exposure is associated with an increased risk of certain cancers, metabolic disorders or reduced fertility, or for phthalates, which can alter the reproductive function.[5] Among MP, antibiotics are a special class that is under particular scrutiny because they can cause antibiotic resistance of microorganisms, thus becoming a major public health problem. Tetracycline (TC) is one of the most widely used antibiotics in medicine and veterinary.[6-7] However, according to the literature, the average rate of TC degradation in wastewater treatment plants is only 30%,[8] explaining its relatively frequent occurrence in surface waters.[9] TC is found at very low concentrations in usual treated wastewaters (from ng L^{-1} to µg L^{-1}), but is sometimes detected at high concentrations in hospital and pharmaceutical effluents (100-500 mg L^{-1}).[10]

In wastewater treatment, high-affinity adsorbents (e.g., activated carbons) are commonly used in polishing treatment to remove residues of undesirable organic chemicals from the aqueous phase. The advantages of adsorption over other processes are that no by-products are formed and a high percentage of undesirable dissolved compounds can be removed from solution.[11] Porous carbon materials have been widely used as effective adsorbents for

antibiotics adsorption (e.g., TC,[10-11] ciprofloxacin,[12] amoxicillin,[13] sulfamethoxazole[14]) due to their large specific surface area, high porosity and favorable pore size distribution. Most of these adsorbents are in the form of particles and most studies have focused on batch reactors. Among antibiotics, TC was one of the most studied.[10-11,15-27] Among adsorbents, activated carbons showed the highest adsorption capacity of TC (from 50 to 800 mg g^{-1} [16, 20] in batch reactors).

Intensification of adsorption processes is about flow configurations because they offer the possibility of reducing costs, operating times, and further automation. A few studies addressed the adsorption of pharmaceutical molecules contained in waters under continuous flow conditions. For TC, it was demonstrated that a good adsorbent in batch process is not automatically a good adsorbent in flow process because of limited diffusion in the pore networks towards the adsorption sites and shorter contact time.[11] Among the activated carbons used in flow, a commercial activated carbon developed by Merck has been found to be the most efficient adsorbent for TC.[11] However, the process can be further improved by optimizing the porosity of the activated carbon, which is of prime importance for efficient use under flow-through conditions.

In this context, we have developed carbon-based adsorbents for wastewater treatment, that are easy to handle and ideal for flow-through processes.[28] Highly porous carbon monoliths (CM) with well-controlled hierarchical micro-/meso-/macropores were obtained by replicating silica monoliths by hydrothermal nanocasting.[28-29] CM proved to be very suitable for high flow, low drop pressure and homogeneous contact time.[28, 30-31] This family of monoliths, prepared by spinodal decomposition,[32] can have different natures (silica, zeolites, titania, etc.) and has proven to be extremely efficient in flow chemistry in many applications such as high performance liquid chromatography and electrochromatography,[33-34] heterogeneous catalysis,[35-40] photocatalysis,[30] biocatalysis,[28, 41-42] oil purification,[43] decontamination of water containing radioactive elements, metal capture,[44-45] etc. In the present study, CM were used to deplete some antibiotics from waters by adsorption under flow. First, the efficiency of these CM was studied with a single antibiotic molecule, i.e., TC. Equilibrium, kinetic and diffusion studies were carried out. Then, CM were used in a batch and in a flow-through configuration for the adsorption of a mixture of antibiotics considered as pharmaceutical MP (i.e., ciprofloxacin, amoxicillin, sulfamethoxazole, tetracycline).

2. Experimental section

2.1 Materials

CM were prepared by replica of silica monoliths (20 µm of macropore and 20 nm of mesopore diameter). Tetraethylorthosilicate (TEOS), polyethylene oxide (PEO, 100 kDa), nitric acid (68%), 3-Aminopropyl triethoxysilane (APTES), sucrose, ciprofloxacin (≥ 98.0 %), amoxicillin (≥ 900 µg mg^{-1}), sulfamethoxazole (≥ 900 µg mg^{-1}) and TC (≥ 98.0 %) were purchased from Sigma Aldrich. Transparent heat shrinkable gains in FluoroEthylenePropylene (FEP AWG ¼" 1.6) with diameters of 6.4 and 3.8 mm before and after shrinkage were purchased from Castello, France.

2.2 Synthesis of silica monoliths

Silica monoliths were synthesized as described in our previous work.[42,46] Deionized water (24.560 g) was poured in 100 mL Erlenmeyer and (2.313 g) nitric acid (68%) was added. The mixture was stirred for 5 min at room temperature. Polyethylene oxide (PEO) of 100 kDa (2.577g) was added and stirred at room temperature until homogenization. The mixture was left at -19 °C for 15 min to cool down the solution without freezing. The Erlenmeyer was then placed in an ice bath and the solution was stirred. Tetraethyl orthosilicate (20 g), previously left 1 h at -19 °C, was directly added to the slurry and stirred for 30 min at 500 rpm to get a homogeneous mixture and a translucent solution. Final composition of the mixture in molar ratio was: 1 Si/ 0.61 EO Unit/ 0.26 HNO_3/ 14.21 H_2O. Polyvinyl chloride (PVC) tubes of 8 mm diameter and 10 cm length were closed on one side with a cap, sealed with parafilm and kept at −19 °C in the freezer. The tubes were removed from the freezer and filled with the mixture from the ice bath. The tubes were then capped and sealed with parafilm and placed in a 4 L water bath at 40 °C for three days. During this time, the phase separation and the sol-gel process took place to form the macroporous network of the monoliths. Then, the monoliths were removed from the molds and placed in a 1 L water bath at room temperature and washed with water until a neutral pH was reached. The monoliths were then immersed in 1 L aqueous ammonia (NH_4OH 0.1 M) in an autoclave and left for 24 h in an oven at 100 °C. The resulting monoliths were placed in a water bath and washed to a neutral pH (1 L of water three times) and then placed in an ethanol bath (500 mL) overnight for solvent exchange. The monoliths were then dried overnight at room temperature and calcined at 550 °C for 8 h at a heating rate of 2 °C min^{-1} from 25 to 550 °C under air to remove residual PEO.

2.3 Synthesis of CM

2.3.1. Synthesis of amino-grafted silica monolith templates

CM were synthesized by replica of silica monoliths using sucrose as carbon source. To favor the adsorption/reaction of sucrose in the mesopores of the silica template, an initial functionalization was carried out by grafting amino groups onto the silica surface. Silica monoliths of 6 mm of diameter and 10 cm long were cut to the desired length (5 mm) using a blade. Then, they were activated at 250 °C in degassing tubes under nitrogen for 6 h to remove the adsorbed water and thus to have a better reproducibility of the grafting. 700 mg of dried silica monoliths were put in contact with 0.838 mL of APTES (corresponding to an excess of 10 moles of APTES per nm^2) in 50 mL of absolute ethanol and allowed to react overnight at 80 °C under reflux. The amino-grafted silica monoliths were then washed with absolute ethanol and dried overnight at 80 °C.

2.3.2. Synthesis of CM by replica of amino-grafted silica monoliths

360 mg of amino-grafted silica monoliths were impregnated with 25 mL of sucrose solution (1.26 M). The mixture was transferred in a Teflon-lined autoclave and a two-step hydrothermal treatment was performed: a first step at 110 °C for 2 h for a better homogeneous impregnation of sucrose into the mesopores and a second step at 180 °C for 16 h for sucrose dehydration and polycondensation to obtain a hydrochar (highly oxygenated hydrothermal carbon) coating into the silica monoliths.[29] The silica/hydrochar composite monoliths were then pyrolyzed under inert atmosphere (Ar, 250 mL min^{-1}) for 2 h at 150 °C, 2 h at 350 °C, 2 h at 550 °C and 6 h at 950 °C with a ramp of 2 °C min^{-1}. Oxygen-poor silica/carbon composite monoliths were then obtained. Finally, the monoliths were washed with a solution of NaOH (2 M) for 24 h at 100°C to remove the remaining silica and obtain carbon monoliths, which were noted as follows CM.

2.4 Characterization methods

Nitrogen sorption isotherms at 77 K were run to analyze the micro- and mesopore surface areas and volumes of CM using a Micromeritics Tristar 3020 apparatus. CM (50 mg) were degassed for 12 h at 80 °C prior to nitrogen sorption analysis. Specific surface area was determined using the BET method. The relative pressure range to use the BET equation was determined with the superior limit given by the maximum of the Rouquerol curve.[47-48] Mesopore diameters were calculated according to the Broekhoff and De Boer (BdB) desorption method[49] at the inflexion point of the desorption step, since it was demonstrated to be one of the most reliable methods for mesoporous materials.[50] Micropore volume and micropore size distribution were

determined by NLDFT analysis of nitrogen adsorption isotherm with SAIEUS software using carbon, slit-shaped pores (2D), and heterogeneous surface area as parameters.

Mercury porosimetry was carried out with a Micromeritics Autopore 9220 equipment by increasing the pressure from 0.0013 to 400 MPa. The mercury intrusion was performed with a monolith of 0.6 cm diameter and 1 cm length. Prior to measurement, the sample was degassed at room temperature for 10 min. The meso- and macropore diameters were determined using the Washburn-Laplace equation (Eq. 1):

$$r = -\frac{2\gamma \cos\theta}{p_{int}} \qquad (1)$$

with r the pore radius, θ the contact angle of mercury with the surface of the pore, γ the surface tension of mercury and p_{int} the pressure of intrusion. The mercury contact angle θ was set at 140° and the mercury surface tension γ at 0.485 N m^{-1}. The macro- and mesopore specific surface areas were calculated by mercury intrusion as shown previously.[45,51]

CM were characterized by scanning electron microscopy (SEM) (Hitachi S-4800 I FEG-SEM) to evidence their interconnected homogeneous network of macropores. The mesopores size and shape were examined using transmission electron microscopy (TEM). TEM micrographs were recorded in transmission mode on a JEOL 1200 EX II microscope operating at 120 kV, from the MEA platform, Univ. Montpellier.

3D imaging of the macroporous network of the monolith was performed by X-ray micro computed-tomography (micro-CT) with a microXCT-400 system (Zeiss). A CM cylinder of 0.6 cm in diameter and 0.5 cm in length was scanned to assess its 3D structure. High resolution scans were acquired at 40 kV and 250 µA. A total of 3001 projections were collected through 360° sample rotation with an exposure time of 20 s per projection. A x 40 magnification optical objective was selected to achieve an isotropic voxel of 0.5 µm and a field-of-view (FOV) of 0.5 × 0.5 × 0.5 mm^3. Volume reconstruction was performed with XM Reconstructed-Parallel Beam-9.0.6445 software using a filtered back projection algorithm.

ORS Dragonfly (version 2020.2 Build 941, Montreal, QC, Canada) software was used for visualization, processing, and analysis of the reconstructed dataset. A cropped sub volume of size 524x594x936 pixels (i.e., 262x297x468 μm^3) was extracted for reasonable calculation time. The procedure for the analysis of the cropped sub volume is detailed below and in the **Figure S1**. First, an automatic Otsu's method segmentation was applied to isolate both the (macro)pore network (void space) and the monolith phase (solid skeleton). Two binary volumes were

obtained, one showing the organization of the (macro)pore network and the second showing the solid phase skeleton. The (macro)porosity was expressed as the ratio of the void space volume to the total volume.

There are three different methods to analyze the generated binary volumes: the "Thickness Mesh" method, the "Dense graph" method and the "Volume thickness Map" method.

The "Thickness Mesh" method produces what is called the "wall thickness quantification" and was performed by computing and generating color-coded mesh for the two binary volumes. A mesh is a collection of vertices, edges, and faces that can define 3D surface geometries in solid modeling. The module "Thickness Mesh" of ORS Dragonfly produces a new mesh object from a binary volume. This mesh provides the "wall thickness measurement" at every surface vertex. "Thickness" is then calculated as the diameter of a hypothetical sphere that fits within two points of the surface.

The "Dense graph" method replaces the network of the binary volume by an assembly of segments. The 3D network modeling was performed for the two binary volumes using the ORS Dragonfly module called "Dense graph". This module creates a skeleton Graph data structure from a binary volume. In a nutshell, it tries to finite it down to a very thin skeleton and then trace a Graph along the binary volume. The obtained network model is a set of nodes connected by edges. Every voxel that was contributed to the graph gets its own node. When a node forks, it forms a branchpoint (i.e., node with a connectivity > 2). A segment is defined as the shortest path between two branchpoints. Scalar values of each segment, such as its length or its tortuosity, can then be exported. Its tortuosity is calculated as a coefficient over the straight-line path (**Figure S2**). Finally, the tortuosity of the monolith solid skeleton and the (macro)pore network can be assessed. Paths from the input (red volume in **Figure S1**) of the network model to the output (green volume in **Figure S1**) are identified and the tortuosity is calculated for each path.

The "Volume thickness Map" method (**Figure S3**) creates a grayscale image/dataset, of which each voxel has an intensity indicating the local "wall thickness" at the location of that voxel. Measurements of volume thickness are based on the sphere-fitting method. The local thickness for a point in pore network or solid skeleton is defined as the diameter of the largest sphere which fulfils two conditions: (i) the sphere encloses the point, but the point is not necessarily in the center of the sphere, and (ii) the sphere is entirely bounded within the solid surfaces.

Zeta potential was measured using a Zetasizer Nanoseries apparatus from Malvern Instruments, pouring crushed CM (5 mg) into 2.5 mL of solution with varying pH values from 2 to 11. After

stirring the suspension for 5 min the potential was measured and plotted as a function of the initial pH of the solution.

XPS measurements were carried out with an ESCALAB 250 instrument of Thermo Electron with an excitation source Al Kα at 1486.6 eV. The analyzed surface had a diameter of 400 µm. The energy was calibrated with the component C=C C 1s at 284.4 eV. N, C, H, O chemical analysis were carried out with "Elementar Vario Micro Cube" analyzer.

TGA was performed using a Perkin Elmer STA 6000 to determine the thermal stability of CM. 10 mg of sample was heated from 40 to 900 °C at a heating rate of 10°C/min under air flow.

2.5 Permeability measurements

Permeability tests were conducted using the same protocol as previously shown for silica monoliths[42,46] by flowing water through CM cladded with a heat shrinkable FEP gain heated at 180 °C for 2 h. CM of 6 mm diameter and 5 mm length were connected to a HPLC pump and a pressure gauge. The flow rate was varied from 0.5 to 10 mL min^{-1}. The permeability was calculated using the Darcy equation (Eq. 2):

$$K = \frac{Q}{A}\frac{l}{\Delta P}\mu \qquad (2)$$

With K permeability coefficient (m^2), Q the flow rate (m^3 s^{-1}), A the cross section of the monolith (m^2), µ is the viscosity of the fluid (µ = 1.002 mPas at 20 °C for water), l the length of the monolith (m) and ΔP is the difference of pressure at the outlet and inlet of the monolith (Pa).

2.6 Adsorption of antibiotics in batch

Adsorption isotherms of TC over CM were carried out with 15 mg (W) of crushed CM added in 40 mL (V) of TC solutions at different initial concentrations (C_0) from 5 to 200 mg L^{-1} prepared in osmosed water (pH 6). After magnetic stirring at 450 rpm for 24 h in a thermostatic shaker bath set at 25 °C, the suspension was filtered and the concentration of TC in the supernatant was measured. The concentration (C_e) of the remaining TC in the solution was analyzed using a UV–Vis spectrophotometer (UV-1800, Shimadzu) at a fixed wavelength of λ = 357 nm. The equilibrium adsorption capacity q_e (mg g^{-1}) was calculated by the equation (Eq. 3) below:

$$q_e = \frac{(C_0 - C_e) \times V}{W} \quad (3)$$

with C_0 and C_e (mg g^{-1}) the initial and equilibrium concentrations of TC, respectively, V (L) the volume of the solution and W (mg) the weight of the adsorbent.
The kinetic of adsorption of TC in CM was carried out at 25 °C with 15 mg of crushed CM added in 40 mL of TC solutions of 100, 150, 200 mg L^{-1} prepared in osmosed water (pH 6). The suspensions were stirred at 450 rpm and the concentration of TC in solution was measured by UV-Vis within time by taking aliquots of 3 mL with a syringe equipped with a filter at regular intervals of time for 24 h. The adsorption capacity was calculated with Eq. 3.

The effect of temperature on the adsorption process of TC in CM was performed at 15, 25 and 35 °C with 15 mg of crushed CM poured in 40 mL of TC solutions of 100 mg L^{-1} prepared in osmosed water (pH 6). The suspensions were stirred at 450 rpm and the concentration of TC in the solution was measured over time by UV-Vis, using a syringe equipped with a filter to withdraw aliquots of 3 mL at regular intervals over a 24 h period. The adsorption capacity was calculated with Eq. 3.

The adsorption of the mixture of pharmaceutical molecules in CM was performed with 15 mg of crushed CM poured in 200 mL of a solution containing ciprofloxacin, amoxicillin, sulfamethoxazole and TC at a concentration of 20 mg L^{-1} each, prepared in osmosed water (pH 6). The suspensions were stirred at 450 rpm and the concentration of each antibiotic in solution was measured over time by High Performance Liquid Chromatography coupled with Mass Spectroscopy (HPLC-MS), using a syringe equipped with a filter to withdraw aliquots of 3 mL at regular intervals over a 24 h period. The adsorption capacity was calculated with Eq. 3. HPLC-MS was carried out with a Waters 2695 apparatus. The aliquots were injected through a Macherey-Nagel C18 column (50 mm x 2 mm) with a Waters e2695 Separations Module, and the molecules were detected with a Micromass Quattro micro API device.

2.7 Adsorption of antibiotics in flow

The adsorption tests in continuous flow were carried out by passing aqueous solutions of TC or of a mixture of antibiotics through CM previously cladded with a heat shrinkable FEP gain heated at 180 °C for 2 h.

Firstly, the TC adsorption in continuous flow (without recirculation) was carried out with a CM of 6 mm diameter and 3 cm length (m = 150 mg) connected to a HPLC pump. The flow rate was set at 0.5 mL min^{-1}. 4 L of TC solution (10 mg L^{-1}) was passed through CM for 120 h. The concentration of TC in the output solution was measured over time by HPLC-MS, using a syringe equipped with a filter to withdraw aliquots of 3 mL at regular intervals. The adsorption capacity was calculated with Eq. 3.

Secondly, the TC adsorption in recirculation flow mode was carried out with a CM of 6 mm diameter and 5 mm length (m = 25 mg) connected to a HPLC pump. The flow rate was set at 1 mL min^{-1}. In order to determine the maximum adsorption capacity under flow of CM, 100 mL of TC solution (200 mg L^{-1}) was passed through CM for 24 h. The concentration of the remaining TC in solution was measured over time by HPLC-MS, using a syringe equipped with a filter to withdraw aliquots of 3 mL at regular intervals over a 24 h period. The adsorption capacity was calculated with Eq. 3. The regeneration of CM by desorption of TC was carried out by passing 80 mL of HCl (0.1 M) solution through the monolith for 24 h at 25 °C in a recirculating mode. The monolith was then washed with 20 mL of water and dried under air flow. Then, a second run of TC adsorption was carried out with 80 mL solution of TC (200 mg L^{-1}).

Finally, the adsorption of a mixture of antibiotics (ciprofloxacin (331.3 g/mol), amoxicillin (365.4 g/mol), sulfamethoxazole (253.3 g/mol) and TC (444.4 g/mol), 20 mg L^{-1} each) was carried out under flow with recirculation with 200 mL of a solution prepared in osmosed water (pH 6) with a CM of 6 mm diameter and 5 mm length (m = 25 mg) connected to a HPLC pump. The flow rate was set at 1 mL min^{-1}. The concentration of each antibiotic in solution was measured by HPLC-MS within time by taking aliquots of 200 µL at regular intervals of time for 24 h. The adsorption capacity was calculated with Eq. 3.

All adsorption measurements in batch and in flow were repeated 3 times, the points reported on the Figures are the average of the 3 values.

3. Results and discussion

3.1 Characterization of CM

CM were obtained by replicating silica monoliths with a mesopore diameter of 20 nm (monomodal) and a macropore diameter of 20 µm[43] using sucrose as a carbon precursor. The mesopores of the silica monoliths are resulting from an aggregation of silica nanoparticles of

10-15 nm diameter (Figure 4). Sucrose was adsorbed on the surface of the silica nanoparticles. The silica monoliths were initially functionalized by amino groups to guarantee a homogeneous deposition of sucrose at the surface of the silica nanoparticles. Indeed, during hydrothermal treatment occurring at 180 °C and a pressure of 10 bar, the pH of the solution is of 3. At this pH, the carbon precursor at negatively charged, as well as, silica nanoparticles (iosoelectric point, IP = 2)[52] resulting in repulsive bonds. On the contrary, the amino-functionalized silica nanoparticles exhibit positive charges (IP = 5)[52] and carbon precursors interact uniformly with the positive charges of the monolith by electrostatic interactions. After the hydrothermal treatment, in which sucrose underwent dehydration and polycondensation to obtain hydrochar, pyrolysis led to a homogeneous deposit of carbon on the silica skeleton and carbon/silica composite monoliths were then obtained.

The silica component was then removed by dissolution in NaOH solution to yield crack-free CM, preserving the same cylindrical shape, diameter, and length as the original silica monoliths. SEM images of CM (**Figure 1**) show that the internal structure has the same homogeneous macropores network as that of the parent silica monolith.[42]

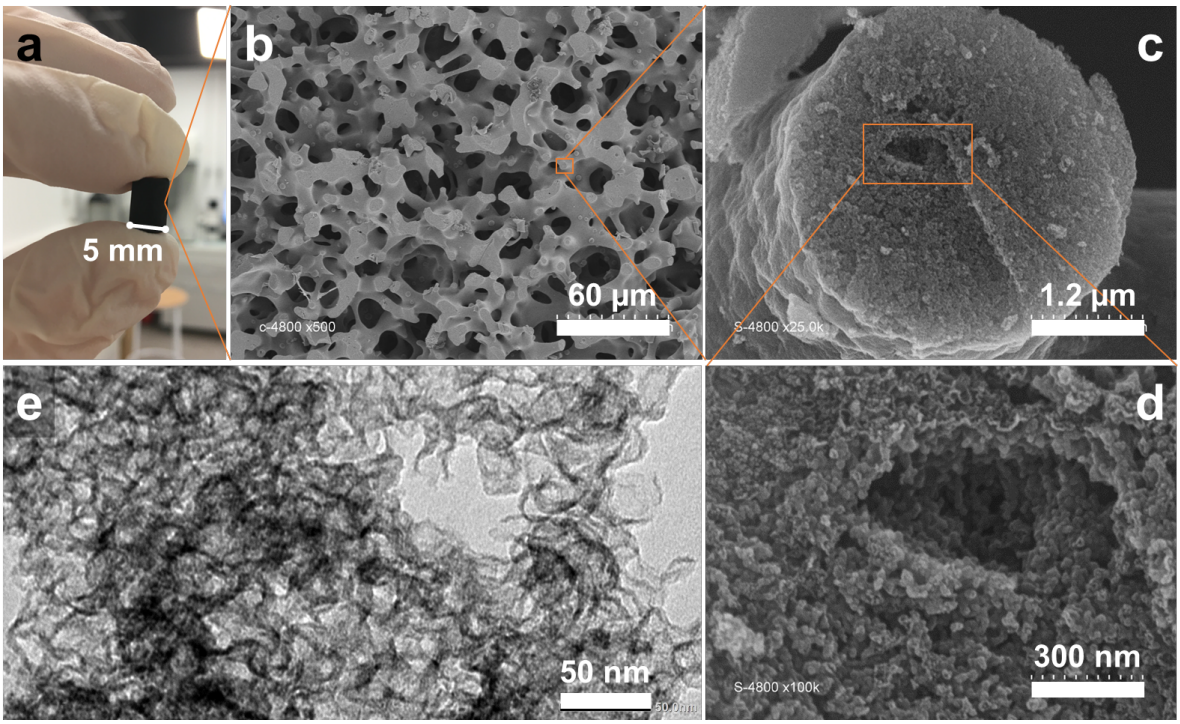

Figure 1. (a) Photograph of a carbon monolith (CM); SEM images of (b) the macroporous network, (c) the carbon skeleton and (d) the mesoporous network inside the carbon skeleton; (e) TEM image of the mesoporous network inside the carbon skeleton.

Based on SEM pictures (**Figure 1b-d**) the macropore diameters of CM are between 7 to 25 µm and the solid skeleton thickness between 4 to 11 µm. The skeleton is built by an aggregation of nanoparticles of 18-22 nm giving rise to ellipsoidal pores of different size (such as 15 x 30 nm, 20 x 70 nm, 40 x 70 nm) in between nanoparticle aggregates (**Figure 1d**). TEM pictures (**Figure 1e**) reveal that the nanoparticles are hollow with a 3 nm shell thickness and an inner diameter around 13-17 nm and can be described as nanocapsules. Some of these nanocapsules are opened or interconnected to others through pore openings of 4-8 nm diameter. Some larger pores (30 x 70 nm) are also identified in between nanocapsule aggregates as observed by TEM and SEM.

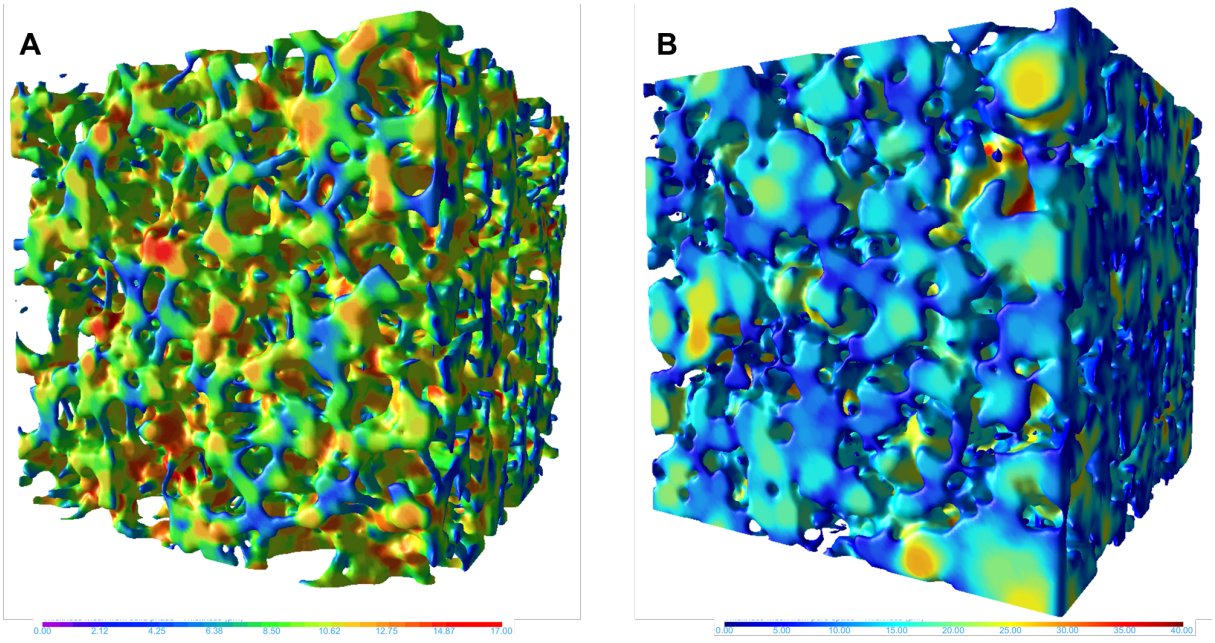

Figure 2. Color-coded "thickness mesh" of (A) the solid skeleton and (B) the (macro)pore network of CM. The meshes are calculated from 3D image (micro-CT) and show the local "wall thickness" at every surface vertex, i.e. the local thickness between boundary points.

CM were further analyzed by 3D imaging by X-ray micro-computed tomography (micro-CT) to assess the structural parameters of the solid skeleton and the (macro)pore network (procedure detailed in **Figure S1**). Micro-CT provides the advantage to characterize the structure in 3D and in a relatively large volume (262x297x468 μm^3) compared to SEM 2D observations and measurements. Results are given in **Table 1** and in **Figures S4 and S5**.

The local "wall thickness" determined by the "Thickness mesh" method of the solid skeleton is between 5 and 15 µm, with an average value of 9.6 µm (**Figure S4**). The evaluation of the

largest spheres that can fit in the solid skeleton ("Volume thickness Map" method) is between 4 and 14 μm, with an average value of 9.2 μm (**Figure S5**). Both methods gave the same results in accordance with SEM observations. The solid skeleton was also modelled into a 3D network model ("Dense graph" method), and is composed of a set of branchpoints connected by 395393 segments. The length of the segments is between 1 and 50 μm with an average value of 20 μm (**Figure S4**). The solid skeleton model exhibits 306 paths from the input to the output (**Figure S1**) with an average tortuosity of 1.46.

The (macro)pore network of CM is homogeneous (**Figure 2**). The calculated (macro)porosity is 65%. The local "wall thickness" determined by the "Thickness mesh" method of the (macro)pore network is between 2 and 34 μm, with an average value of 14.3 μm (**Figure S4**). The evaluation of the largest spheres that can fit in the macropores ("Volume thickness Map" method) is between 3 and 34 μm, with an average value of 19.7 μm (**Figure S5**). Whereas the results obtained by the two methods ("Thickness mesh" and "Volume thickness map" methods) are identical for the solid skeleton analysis, they differ for the macropore network description (**Figures S4 and S5**) due certainly to a larger distribution of pore size in comparison to the skeleton thickness. The obtained (macro)pore network was also modelled by the "Dense graph" method and consists of branchpoints with an average connectivity of 3.2 connected by 464864 segments with an average length of 18.9 μm. The (macro)pore network model exhibits 306 paths from the input to the output with an average tortuosity of 1.48.

Similar analysis carried out on the parent silica monolith[42] showed a good agreement between 3D structural parameters of silica monolith and CM (**Table 1, Figures S4 and S5**). It shows that the carbon precursors were adsorbed and coated only in the mesopores of the silica monolith and did not affect the macropore network.

Table 1. Structure parameters of the solid skeleton and the (macro)pore network obtained from 3D images of CM and parent silica monolith (micro-CT). The 3D image analyze procedure is detailed in **Figure S1**.

	Parent Silica Monolith	**CM**
Solid Skeleton		
Thickness mesh		
Mean "local wall thickness" (μm)	9.7	9.6
Volume thickness map		
Sphere diameter (μm)	9.5	9.2

Network modeling (Dense graph)		
Number of segments	390441	395393
Mean segment length (μm)	19.5	20
Mean segment tortuosity	1.2	1.2
Number of branchpoints	15879	15564
Mean branchpoint connectivity	3.5	3.3
Tortuosity (number of paths from input to output)	1.46 (400)	1.46 (306)
(Macro)pore network		
Porosity ε_{macro}	0.65	0.65
Thickness mesh		
Mean "local wall thickness" (μm)	14.2	14.3
Volume thickness map		
Sphere diameter (μm)	19.5	19.7
Network modeling (Dense graph)		
Number of segments	467102	464854
Mean segment length (μm)	18.5	18.9
Mean segment tortuosity	1.2	1.2
Number of branchpoints	18057	17566
Mean branchpoint connectivity	3.2	3.2
Tortuosity (number of paths from input to output)	1.47 (380)	1.48 (306)

Mercury porosimetry (**Figure 3**) was carried out to analyze both the macropore and the mesopore networks of CM. It is to recall that Hg cannot penetrate in pores smaller than 4 nm diameter. The Hg intrusion curve shows two distinct steps at low and high pressure confirming the hierarchical porosity (macro- and mesopores) of CM with a narrow macropore diameter distribution centered at 22.5 μm corresponding to a macropore volume V = 4.5 mL g^{-1}. Good agreement is found between average macropore diameter determined by Hg porosimetry (22.5 and 21.2 μm for CM and silica monolith,[42] respectively) and micro-CT with "Volume thickness Map" method (19.7 and 19.5 μm for CM and silica monolith, respectively). An excellent agreement between Hg porosimetry and micro-CT could be assessed if contact angles of 132° and 135° for CM and silica monolith, respectively, are taken instead of 140° in the Washburn-Laplace equation (Eq.1). Contact angle values of 131° are recommended for silica surface[53] and 150-163° for carbon surface.[51] A contact angle of 132° for CM would indicate that CM has a more oxide-like surface behavior compared to activated carbons. The macropore diameter D can be also estimated by the Gurvitch equation (D = 4V/S) assuming cylindrical pores from the

specific surface area S of the macroporous network of CM. The calculation by Hg porosimetry of CM surface area gives S = 0.89 $m^2 g^{-1}$, which leads to a mean pore diameter of 20.2 µm in agreement with the Washburn-Laplace pore size distribution and the micro-CT by "Volume thickness Map" method.

The "total" porosity (including the meso- and the macropores) of CM determined by Hg porosimetry is 82%, and 62% for the porosity of the sole macropores (in agreement with micro-CT which gives 65%). The density of CM determined by Hg porosimetry is 0.142 g cm^{-3}. Therefore the macropore volume (4.5 mL g^{-1}) expressed per volume of monoliths (0.64 mL cm^{-3}) is similar to the one of the parent silica monolith (0.65 mL cm^{-3}, 0.1875 g cm^{-3}). The specific surface area of the macroporous network of CM (0.89 $m^2 g^{-1}$) determined by Hg intrusion expressed per volume of monoliths (0.126 $m^2 cm^{-3}$) is similar as the one of the parent silica monolith (0.67 $m^2 g^{-1}$, 0.126 $m^2 cm^{-3}$). During replication, only the mesopore network was replicated, the macropore network is the same as that of the parent silica monolith, as previously observed by micro-CT.

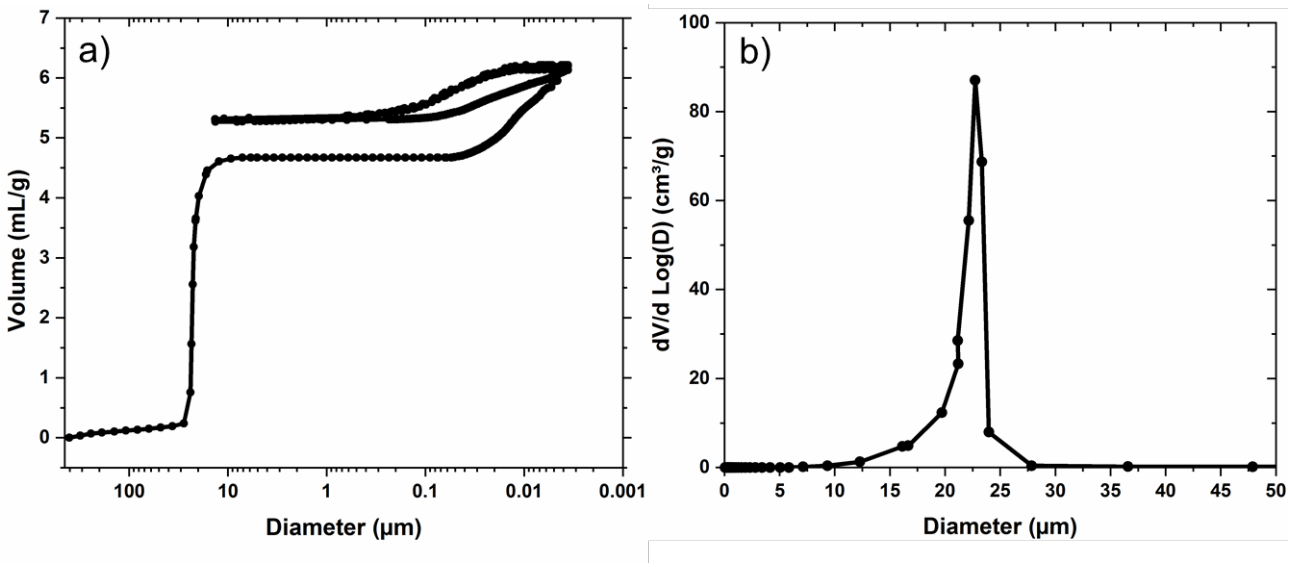

Figure 3. (a) Mercury porosimetry of CM and (b) macropore size distribution. The pore diameters were determined by the Washburn-Laplace equation (Eq. 1).

Hg porosimetry of CM shows that mesopores feature a large distribution of pore diameters from 3 to 46 nm corresponding to a total mesopore volume of 1.62 mL g^{-1} accessible to Hg. The second run of Hg intrusion/extrusion is not superposing the first run, suggesting that some mercury remains trapped in some mesopores due to constrictions. A volume of 0.84 mL g^{-1} of mesopores (from 3 to 50 nm diameter) is freely accessible to successive intrusion of mercury.

The intrusion curve shows two steps in the mesopore domain: (step 1) from 35 to 10 nm (0.84 mL/g) and (step 2) from 10 to 3 nm (0.78 mL/g). The first step can be attributed to the large ellipsoidal mesopores observed by SEM and TEM (**Figure 1**), whereas the second step should correspond to the filling of the nanocapsules observed by TEM. The large hysteresis indicates the presence of constricted mesopores (bottleneck-like mesopores)[54] certainly due to the nanocapsules. In this case, Hg intrusion is driven by the constrictions and lead to a two steps mechanism explaining the complex shape of the intrusion curve. The diameter of the constriction could be estimated by the step at the higher pressure (~5 nm). The diameter of the cavity can be estimated by applying the Washburn-Laplace equation for intrusion (Eq. 1) to the first pressure of extrusion (~15 nm). This result is in good agreement with the size of the nanocapsules observed by TEM (cavities of 13-17 nm with opening windows of 4-8 nm) (**Figure 1**). The specific surface area of the mesopores of CM determined by Hg intrusion for mesopore diameters from 3 to 50 nm is 475 m^2 g^{-1}.

The mesopore network of CM was also analyzed by nitrogen adsorption/desorption isotherm at 77 K (**Figure 4, Figure S6**).

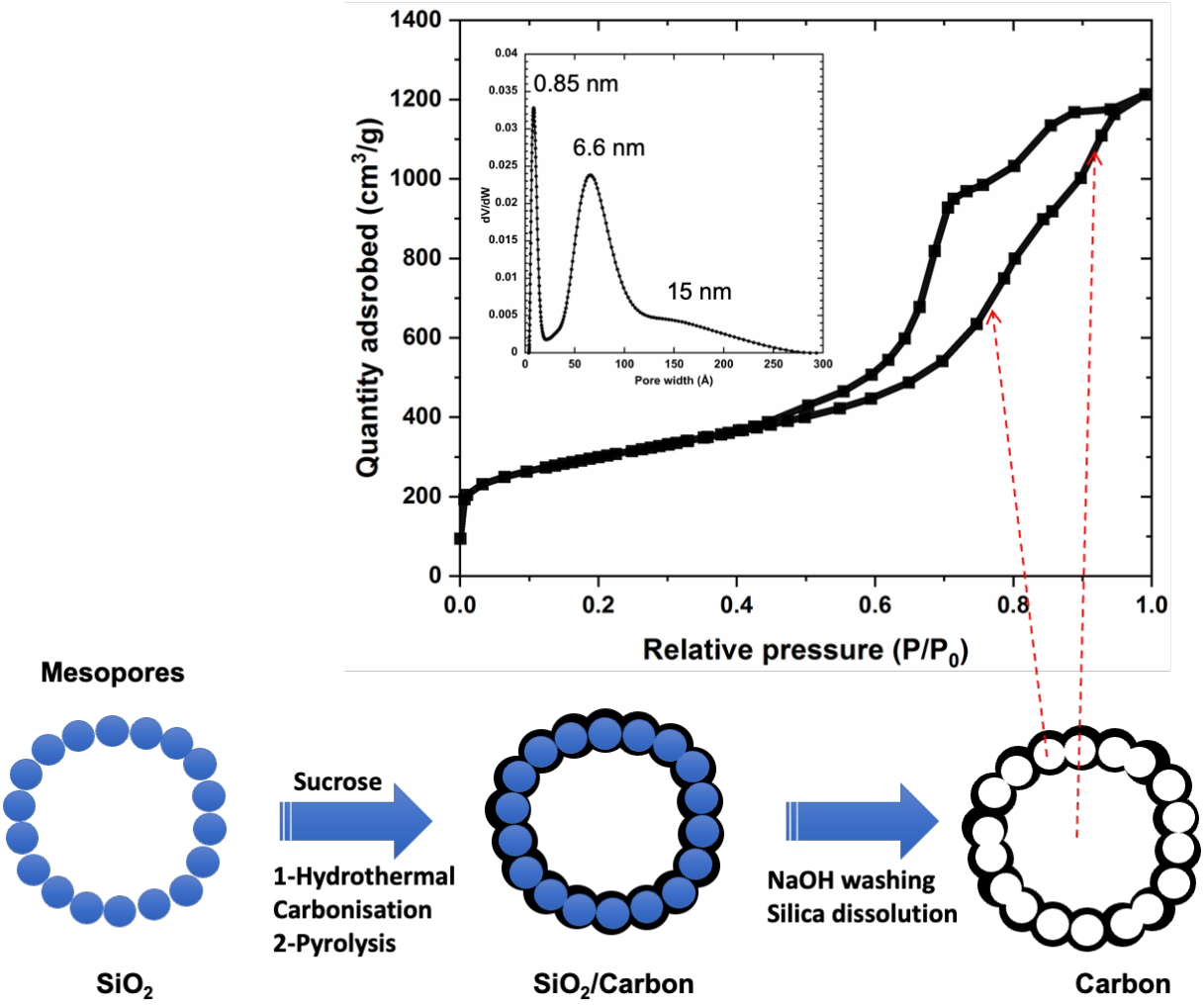

Figure 4. (up) Nitrogen sorption isotherm at 77K of CM and (down) schematic representation of the origin of the bimodal mesoporosity of CM (large ellipsoidal mesopores and nanocapsules) coming from the replica of the silica monolith with monomodal mesopore network (20 nm diameter) formed by an aggregation of silica nanoparticles of 10-15 nm (in blue) on which carbon (in black) has been deposited to form silica nanoparticles surrounded by a carbon layer. Then, the removal of silica by NaOH washing results in empty nanocapsules of carbon (inducing a new smaller mesoporosity) together with the original large mesopores of the parent silica monolith. Inset: Micro-/mesopore size distribution of CM with software SAIEUS with the model of carbon 2D heterogeneous surface, N_2 at 77 K from cumulative pore volume.

The total specific surface area calculated from the nitrogen adsorption isotherm is S_{BET} = 1058 $m^2\ g^{-1}$, which is much higher than the mesopore surface area of CM determined by Hg porosimetry (475 $m^2\ g^{-1}$) for pores with diameter in the range 3-50 nm. This result suggests the presence of micropores in CM. The analysis of the nitrogen isotherm by NLDFT and

cumulative pore volume indeed shows the presence of micropores with a pore width of about 0.85 nm, giving a micropore volume of 0.24 mL g^{-1} and a micropore surface area of 522 m^2 g^{-1} (**Figure S6**). By difference with the total surface area, the mesopore surface area is 536 m^2 g^{-1}, which is slightly higher but close to the one determined by Hg intrusion (475 m^2 g^{-1}). A part of the mesopores of the nanocapsules might not be accessible by Hg. The nitrogen adsorption isotherm shows two steps confirming the presence of two kinds of mesopores: small mesopores (4-19 nm) and large mesopores (> 19 nm). The analysis of the isotherm is complex. The pore volume of the larger mesopore cannot be calculated as the isotherm suggests the presence of larger pores than 30 nm that cannot be filled by N_2 adsorption at 77 K. The smaller mesopores are constricted pores[55] (corresponding to the nanocapsules) with an estimated cavity size of about 11.2 nm and constrictions of about 4.4 nm in agreement with TEM observations (**Figure 1**). The pore volume at the end of the filling of the small mesopores is 1.50 mL g^{-1} ($p/p_0 = 0.77$). By subtraction of the micropore volume (0.24 mL g^{-1}), the volume of the smaller mesopores is estimated at around 1.26 mL g^{-1}.

The combination of all the characterization technics allows describing the hierarchical porosity of CM (**Table 2**).

Table 2. Textural properties of CM

Pore Types	Pore Diameter	V (mL g^{-1})	S (m^2 g^{-1})
Micropores	0.85 nm	0.24	522
Mesoporous nanocapsules	Cavity: 11-17 nm		
	Opening: 4-8 nm	1.26	536[a]
Ellipsoidal mesopores	20-35 nm	0.84	
Macropores	20-22 µm	4.50	0.9
Total		6.84	1058

[a] Specific surface area for all mesopores: nanocapsules and large ellipsoidal mesopores.

The hierarchical porosity (micro-/meso-/microporosity) of CM has been demonstrated. The presence of mesopores in addition of the intrinsic micropores of carbon materials are important to insure no steric hindrance limitation and favors adsorption of large molecules as antibiotics[56] and the presence of macropores allows the use of these monoliths in continuous flow with low pressure drop.

The permeability of CM (6 mm diameter, 5 mm length) was measured using water under continuous flow. Under the experimental conditions, a backpressure was not detectable with

our instrument for flow rates inferior to 4 mL min^{-1}, showing the excellent permeability of CM. For higher flow rates, the pressure drop increased linearly with the increase of flow rate (**Figure 5**), following the Darcy law (Eq. 2) with a permeability coefficient (K) of 3.55 10^{-12} m^2.

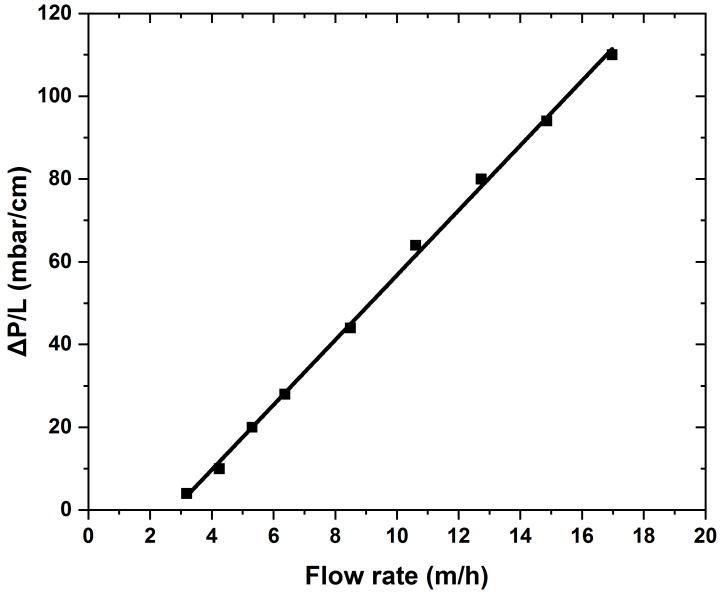

Figure 5. Pressure drop as a function flow rate for CM.

From the Hagen-Poiseuille law, the permeability (average fluid flux times viscosity divided by potential gradient) for steady laminar flow in a permeable medium of diameter D, porosity ε and tortuosity τ, is expressed as[57] (Eq. 4):

$$K = \frac{D^2 \varepsilon}{32\tau} \qquad (4)$$

The permeability coefficient is dependent only of the macropore network: macropore diameter, (macro)porosity and tortuosity. For a complex macropore system as CM (even if it is homogeneous), it is difficult to define a representative diameter. However, by using the structural parameters calculated by micro-CT (ε = 0.65, τ = 1.48) (Table 1), the corresponding macropore diameter D calculated from the permeability measurement by Eq. 4 is 16.1 µm, which is in good agreement with micro-CT measurements (14.7 and 19.5 µm for the "Thickness Mesh" and "Volume thickness Map" methods, respectively, 20-22 µm for the Washburn-Laplace pore size distribution (depending on the contact angle) and 20 µm for the Gurvitch method, the last two methods being derived from Hg porosimetry with an assumption of cylindrical pores). The permeability of CM is in agreement with a steady laminar flow in a porous medium of mean cylindrical interconnected portions of diameter 16.1 µm.

It should be noted that to represent a complex permeable medium, the pore diameter is sometimes replaced by the hydraulic radius R_h, which is the ratio of the volume open to flow to the wetted surface area and can be expressed as follows:[57]

$$R_h = \frac{\varepsilon}{(1-\varepsilon)S}$$

By using the (macro)porosity calculated by micro-CT (ε = 0.65) and the specific surface area of macropores per volume determined by Hg porosimetry (S = 0.126 m^2/cm^3) for CM, R_h is equal to 14.7 μm, which is equal to the value found by the "Thickness Mesh" method of micro-CT to described the macroporosity of CM.

The chemical analysis of CM yielded the following composition: 87.99 wt% C, 8.16 wt% O, 1.07 wt% H, 1.16 wt% N, corresponding to O/C = 0.07 (at/at), H/C = 0.146 (at/at), N/C = 0.01 (at/at). XPS measurements confirmed the low oxygen content (0.06 at%) of CM and revealed the nature of the carbon: C=C 74 at%, C-C 10 at%, C-O 6 at%, C=O 2 at%, COO^-, COOH,R 8 at % (**Figure S7**). The presence of N (coming from amino-grafted silica precursor) might be responsible for the basic character of CM. The zeta potential measurements show that CM have a pH of the point of zero charge, pH_{pzc}, of 3 and hence a negatively charged surface in aqueous solutions with a pH > 3 (**Figure S8**), presumably due to the presence of a large amount of COO^- species in comparison to activated carbon (**Table S1**). A suspension of CM in water (with an initial pH of 6) increased to a pH of 9, showing that CM are basic adsorbents.

In addition, TGA showed that CM are stable in air flow until 400 °C (**Figure S9**).

3.2 Adsorption of TC on CM

Prior to study the depletion of waters containing several antibiotics, the behavior of CM as adsorbent was analyzed with a single pharmaceutical molecule, TC (**Figure S10**). This molecule was chosen as it is one of the most studied in literature[11,15-20] to analyze the sorption capacity of materials, as well as kinetics and diffusion phenomena. TC molecule is zwiterionic at pH 6 and becomes negatively charged at pH 9 (**Figure S10**). The molecule size is around 0.85 nm x 1.25 nm. TC has a general structure known as 1,4,4a,5,5a,6,11,12a-octahydronaphtacene formed by four condensed rings consisting of six atoms each (**Figure S10**).[58] The TC molecule has three dissociable protons corresponding to (1) the deprotonation of tricarbony-methane group (pKa_1 = 3.3) (corresponding to the equilibrium between the forms

TCH_3^+ and $TCH_2°$), (2) the deprotonation of ketophenolic hydroxyl group (pKa_2 = 7.68) (corresponding to the equilibrium between the forms $TCH_2°$ and TCH^-), (3) the deprotonation of the dimethylamino group (pKa_3 = 9.69) (corresponding to the equilibrium between the forms TCH^- and TC^{2-}) (**Figure S10**). The three forms TCH_3^+, $TCH_2°$, TCH^- feature the protonated dimethylamino group ($N^+(H)(CH_3)_2$), whereas TC^{2-} has no positive charge, only negative charges, which would give electrostatic repulsion with the negatively charged CM surface. The initial pH of the TC solution in osmosed water was pH 6 and it rose to pH 9 with the addition of CM. At pH 9, 86% of TC molecules would contain the positively charged $N^+(H)(CH_3)_2$ group (**Figure S10**): $TCH_2°$ (4.4%), TCH^- (81.5%), TC^{2-} (14.1%).

3.2.1 Adsorption of TC on CM in batch

3.2.1.1 Adsorption isotherm of TC on CM

The adsorption isotherm of TC on CM (**Figure 6**) is of type L[59] characteristic of adsorbents with a high affinity for the adsorbate. The adsorption capacity increases with the increase of the equilibrium concentration. When the initial TC concentration is lower than 120 mg L^{-1}, the final equilibrium concentration is lower than 9 mg L^{-1} corresponding to removal efficiencies higher than 92.5%. Adsorption isotherms can be described by many models, some based on a simplified physical description of adsorption, while others are purely empirical and are intended to correlate experimental data.

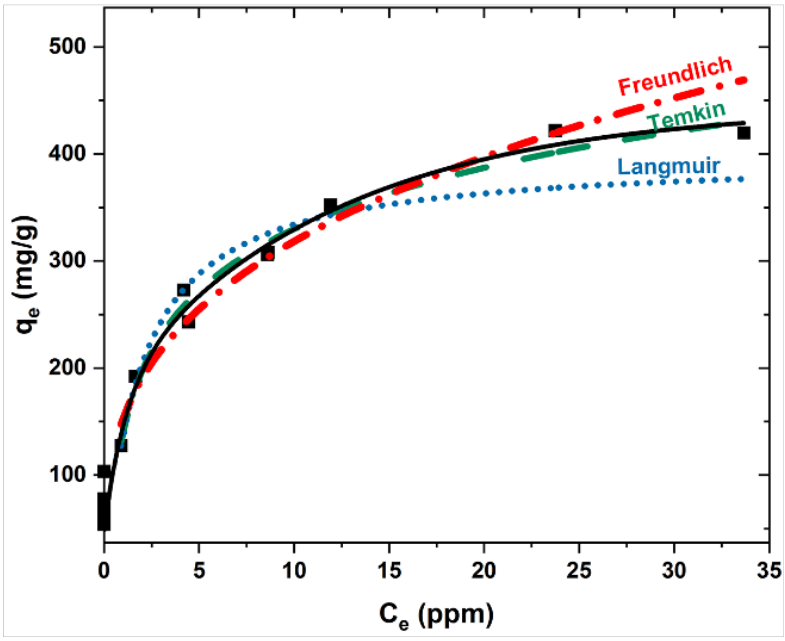

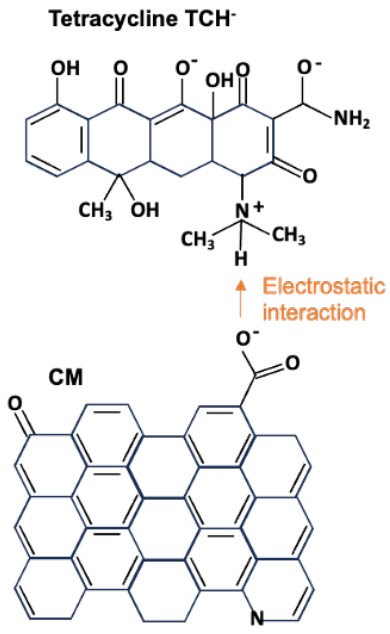

Figure 6. (left) Adsorption isotherm of TC in CM in batch: (squares and continuous black line) experimental data compared to the fits of (doted lines) (blue) Langmuir, (red) Freundlich and (green) Temkin models. Experimental conditions: pH 6; T = 298 K; time = 24 h; CM 375 mg L^{-1}. (right) Schematic representation of adsorption mechanism of TC on CM.

In this study, three different models Langmuir,[60] Freundlich[61] and Temkin[62] were used to analyze the adsorption isotherm (**Figure 6, Table 3**). The deviation of the experimental data from the models were calculated by the normalized standard deviation parameter Δq_e (%) with the following equation (Eq. 5):

$$\Delta q_e(\%) = 100\sqrt{\frac{\Sigma[(q_{e,exp} - q_{e,cal})\backslash q_{e,exp}]^2}{(N-1)}} \qquad (5)$$

where N is the number of experimental data, $q_{t,exp}$ and $q_{t,cal}$ (mg g^{-1}) are experimental and calculated adsorption capacity, respectively.

The fits between the three models and the experimental results are shown in **Figure 6** and the calculated parameters are listed in **Table 3**.

Table 3. Parameters of the three different models (Langmuir, Freundlich and Temkin) used to fit the adsorption isotherm of TC on CM.

Model	Langmuir	Freundlich	Temkin
Equation	$q_e = q_m \times \frac{K_L C_e}{1 + K_L C_e}$	$q_e = K_F C_e^{1/n}$	$q_e = \frac{RT}{b_T} \times \ln(K_T C_e)$
Linearization	$\frac{1}{q_e} = \frac{1}{q_m \times K_L \times C_e} + \frac{1}{q_m}$	$\ln(q_e) = \frac{1}{n_F}\ln(C_e) + \frac{1}{n_F}\ln(K_F)$	$q_e = \frac{RT}{b_T}\ln(K_T) + \frac{RT}{b_T}\ln(C_e)$
R^2	0.9755	0.9527	0.9796
Parameters	$q_m = 400$ mg g^{-1} $K_L = 0.52$ L mg^{-1}	$K_F = 152.50$ mg g^{-1} $n_F = 3.13$ $1/n_F = 0.32$	$b_T = 29.93$ J mol^{-1} $K_T = 5.38$
Conclusion	Maximum adsorption capacity: 400 mg g^{-1} The hypothesis of homogenous sites of adsorption is limited.	$n_F > 1$: physical adsorption $1/n_F$ close to 0: Heterogeneous sites of adsorption	$b_T > 1$: exothermic adsorption Electrostatic interaction Heterogeneous sites of adsorption Adsorption energy decreases with the surface coverage
Δq_e (%)	6.21	6.24	3.59

q_m: theoretical maximum adsorption capacity per unit mass of CM (mg g^{-1}); K_L, K_F and K_T: adsorption constants of Langmuir, Freundlich and Temkin, respectively; n_F: Freundlich linearity index; b_T: energy of adsorption.

The Temkin model has the highest correlation coefficient ($R^2 = 0.9796$) (**Figure S11**) and the lowest deviation from the experimental data ($\Delta q_e = 3.59\%$). The Temkin model is the most suitable to represent the adsorption isotherm of TC on CM. This indicated that: (i) the sites of adsorption are heterogeneous, (ii) the adsorption is exothermic,[63] (iii) the adsorption energy decreases linearly with the surface coverage due to adsorbent-adsorbate interactions, (iv) the interactions are electrostatic.[64] This model is also the best to describe TC adsorption in some activated carbons as the one issued from macadamia nut shell.[17] According to the authors,[17] this suggests that there are electrostatic interactions between the adsorbate and the adsorbent and that surface heterogeneity plays an important role in TC adsorption. The value of the n_F parameter of the Freundlich model is 3.13 and the $1/n_F$ ratio gives information about the surface heterogeneity. The closer the ratio $1/n_F$ is to zero, the more heterogeneous the surface of the adsorbent is.[65] A $1/n_F$ ratio of 0.34 for CM indicates that the adsorption sites are heterogeneous, but less heterogeneous than those of the commercial activated carbon from Merck ($1/nF = 0.10$)[11] or from petroleum coke ($1/n_F = 0.077$).[16] The maximum adsorption capacity of TC on CM (400 mg g^{-1}) was calculated by the Langmuir equation (**Table 3**). We observed that it is close to the adsorption capacity of some activated carbons as the one commercialized by Merck

(470 mg g^{-1})[11] and an activated carbon issued from macadamia nut shell (460 mg g^{-1})[17] (**Figure 7**), but it is lower than some others as the one issued from sludges (510-670 mg g^{-1})[11] or from petroleum coke (810 mg g^{-1})[16] (**Figure 7**).

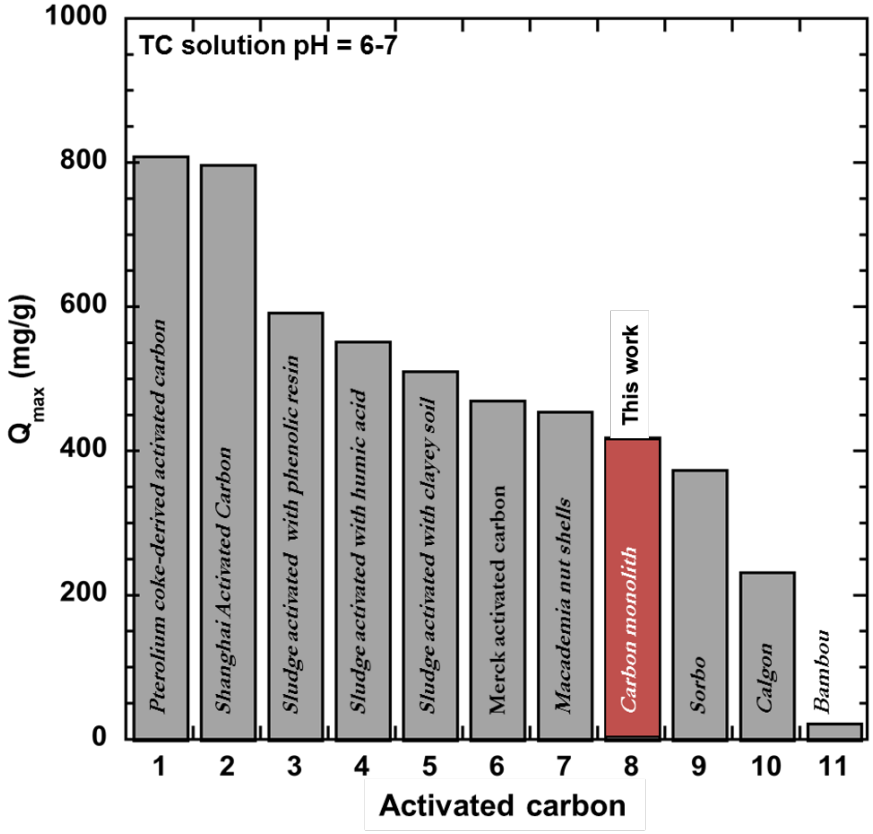

Figure 7. Maximum adsorption capacity in batch of TC on CM and on different activated carbons, calculated by the Langmuir equation. The x-axis represents the different types of activated carbon (AC), the values are taken from the literature: (AC1) from ref.[16], (AC2) from ref.[20], (AC3, 4, 5, 6, 9) from ref.[11], (AC7) from ref.[17], (AC8) from this work, (AC10) from ref.[66], (AC11) from ref.[19].

It was demonstrated that a good adsorbent in batch is not systematically a good adsorbent in flow due to diffusion limitations in the pore networks towards the adsorptive sites and to the shorter contact time.[11] The commercial activated carbon of Merck (issued from the pyrolysis of coconut shells) was the most efficient in flow (packed-bed columns) in comparison to activated carbons coming from sludges,[11] even though the latter had higher adsorption capacities in batch (**Figure 7**). The porosity and the porosity network of activated carbons are of prime importance for an efficient use in flow conditions. Merck's activated carbon is formed as particles with a diameter of about 1 mm, having a disordered sponge-like macroporous structure with

macropore diameters of 1 to 10 µm and a macropore volume of 0.28 mL g^{-1}. There are few mesopores (0.10 mL g^{-1}) and they feature a wide distribution of mesopore diameters, ranging from 6.6 to 50 nm (**Table S1**). The total intra-particle pore volume is 0.38 mL g^{-1}. The macropore volume is the inter-particle pore volume, i.e., the pore volume between the particles. In a packed-bed column (with a bed diameter larger than 10 times the particle diameter), the (macro)porosity is around 0.36 - 0.43.[67] As for CM, the (macro)porosity is higher (0.65), the macropore network is more homogeneous, and the macro and mesopore volume is higher (**Table 2**). The "intra-particle" (intra-skeleton) pore volume is 2.1 mL g^{-1}, hence five times higher than that of Merck's activated carbon. It has been shown that the diffusion coefficient increases with the increase of intra-particle porosity, especially for a pore diameter seven times larger than the size of the diffusing molecule.[68] Therefore, intra-particular diffusion should be more efficient in CM than in Merck's activated carbon. At first glance, CM should be better adsorbents in flow conditions than Merck's activated carbon due to its porous network (**Table S1**).

Nonetheless, there is a strong difference between the two carbon materials, which is their surface charge: Merck's activated carbon has a pH_{pzc} of 7.7 and CM of 3. At a pH of 6-7, Merck's activated carbon is positively charged, while CM is negatively charged. The pH of their suspension in water is different: pH = 4-5 for Merck's activated carbon and pH = 9 for CM. This difference is probably due to the strong acid treatment before pyrolysis occurring in the preparation of Merck's activated carbon, and the basic treatment by NaOH to remove silica from the monolith to obtain CM, leading presumably to COO^-Na^+ groups in CM surface and COOH groups in Merck activated carbon. The pH of the medium influences the TC charges and therefore the adsorption mechanisms.

3.2.1.2 Adsorption kinetics of TC on CM in batch

In flow processes, only fast reactions proceed. It is therefore important to analyze the adsorption kinetics in batch process to understand the adsorption mechanisms. The kinetics of adsorption of TC on CM was followed with three initial TC concentrations: 100, 150 and 200 mg L^{-1} (**Figure 8**). First, a fast adsorption phase was observed within the first hour, followed by a second slow adsorption phase reaching a plateau after 5 h, which could express the equilibrium between the adsorbed molecules and the ones in solution. In the first hour, the TC adsorption capacity increased from 214 to 270 mg g^{-1} with the increase of the initial concentration from 100 to 150 mg L^{-1}, corresponding to a TC removal of 80 and 67%, respectively. At the highest initial TC concentration (200 mg L^{-1}), the adsorption capacity was also 270 mg g^{-1}, but with a

lower adsorption yield of 51%. The maximum steady-state adsorption capacity after 24 h increased with the initial TC concentration and reached 242, 349 and 420 mg g^{-1} for the initial TC concentration of 100, 150 and 200 mg L^{-1}, respectively, corresponding to a removal of 91, 87 and 79% of TC. Experimental results were compared with kinetic equations representing either the pseudo-first or pseudo-second order reactions (**Figure 8**, **Table 4**).

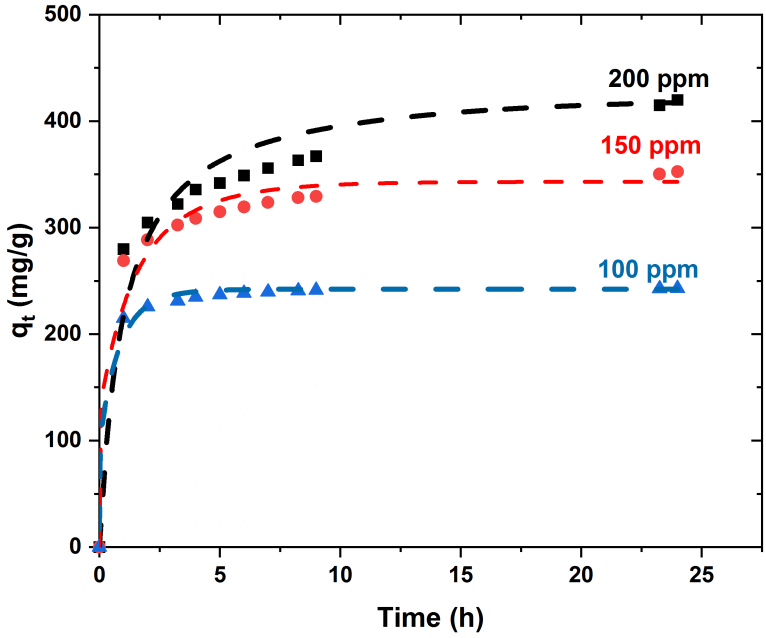

Figure 8. Adsorption of TC in batch as a function of time on CM for three initial TC concentrations: 100, 150 and 200 mg L^{-1}. Experimental conditions: pH = 6, T = 298 K, CM 375 mg L^{-1}. The dashed lines represent the fits by the equation of the pseudo-second order model.

The pseudo-first order kinetic model[69] follows the equation (Eq. 6):

$$\frac{dq}{dt} = k_1(q_e - q_t) \quad (6)$$

corresponding to the linearization (Eq. 7):

$$\ln [q_e - q(t)] = \ln q_e - k_1 t \quad (7)$$

The pseudo-second order kinetic model[70] follows the equation (Eq. 8):

$$\frac{dq}{dt} = k_2(q_e - q_t)^2 \quad (8)$$

corresponding to the linearization (Eq. 9):

$$\frac{t}{q(t)} = \frac{t}{q_e} + \frac{1}{k_2 q_e^2} \quad (9)$$

where k_1 (h^{-1}), k_2 (g mg^{-1} h^{-1}) are the rate constants of the pseudo-first order and the pseudo-second order models, respectively.

Table 4. Kinetic parameters of TC adsorption on CM.

C_0 (mg L^{-1})	*Pseudo-first* order model				*Pseudo-second* order model			
	k_1 10^{-3} (min^{-1})	$q_{e.cal}$ (mg g^{-1})	R^2	$\Delta q(\%)$	k_2 10^{-5} (g mg^{-1} min^{-1})	$q_{e.cal}$ (mg g^{-1})	R^2	$\Delta q(\%)$
100	2.7	109	0.9277	68.50	7.8	208	0.9978	6.27
150	2.9	113	0.8875	78.45	8.7	357	0.9992	4.53
200	2.7	199	0.9313	65.97	3.8	434	0.9982	8.35

The kinetics of adsorption of TC on CM shows a poor correlation ($R^2 < 0.93$) with the pseudo-first order model (**Table 4**). The calculated adsorbed amounts are lower than the experimental data. A very good agreement was found with the pseudo-second order model (**Figure 8, Table 4**). Excellent correlation coefficients ($R^2 > 0.997$) and small deviations between experiment and calculated adsorbed quantities ($\Delta q_e < 8\%$) were found. The adsorbed amounts depend only on the initial concentration and contact time. The calculated adsorbed amounts at equilibrium are close to the experimental values (**Figure 8, Table 4**). The pseudo-second order model was also well suited to follow the adsorption of TC on activated carbons from macadamia nut shells[17] and from petroleum coke.[16]

The initial rate of adsorption of TC on CM was calculated using the following equation (Eq. 10):

$$h_0 = k_2 q_e^2 \quad (10)$$

The initial rate of adsorption increases from h_0 = 3.5 to 11 mg g^{-1} min^{-1} with the increase of the initial TC concentration from 100 to 150 mg L^{-1}, respectively, but then decreases to h_0 = 7 mg g^{-1} min^{-1} for an initial TC concentration of 200 mg L^{-1}. One explanation for this phenomenon

could be that TC molecules initially adsorb rapidly (during the first hour) flat on the surface until the entire surface is covered, corresponding to an adsorption capacity of about 270 mg g^{-1}. Then the molecules rearrange themselves, smoothing the surface with a slow realignment to allow more molecules to access the surface, resulting in an overall lower initial adsorption rate at a very high initial TC concentration. Following this hypothesis, we could predict that the initial fast rate of adsorption would increase as the surface area of the carbon materials increased. This is the case with activated carbon made from coke[16] (initial rate of TC adsorption h_0 = 60 mg g^{-1} min^{-1} at an initial TC concentration of 100 mg L^{-1}), which has a surface area (2200 m^2 g^{-1}) twice that of CM. The rate of adsorption is 17 times faster. This suggests that the mechanism of adsorption differs between these two types of carbon materials, and more generally between activated carbons and CM, presumably due to the basicity of CM and its negatively charged surface.

At pH 5-7, activated carbon surfaces are mostly positively charged ($7 < pH_{pzc} < 10$). The majority of TC molecules are under the form $TCH_2°$, which is zwitterionic ($3.5 < pH < 7.5$), with the positively charged deprotonated dimethylamino group ($N^+(H)(CH_3)_2$) and the negatively charged $C(O^-)NH_2$ group (**Figure S10**).[11] It has been demonstrated that for activated carbons electrostatic interactions are negligible for adsorption at pH 7 and that the main interactions are through π-π or cation-π bonds and predominantly through H-bonds between the –OH and NH_2 groups of TC and the COOH and mainly C=O functions of activated carbon surfaces.[19] For CM, as their surface is negatively charged, it can be suggested that the mechanism of adsorption of TC is different and rather predominantly through electrostatic interactions with the positively charged $N^+(H)(CH_3)_2$ groups of TC molecules. At pH 9, 86% of TC molecules (4.4% $TCH_2°$, 81.5% TCH^-) present the protonated ammonium group $N^+(H)(CH_3)_2$ and 14.1% are as TC^{2-} (**Figure S10**). The rapid adsorption of TC corresponds to about 80% of TC in solution (at an initial concentration of 100 mg L^{-1}), which could correspond to the complete adsorption of the protonated TC molecules ($TCH_2°$ and TCH^-) and no adsorption of the TC^{2-} species containing no positively charged group.

3.2.1.3 Diffusion of TC in CM

To further understand the adsorption process on CM, the kinetics results were also analyzed by the intra-particle diffusion model proposed by Weber and Morris.[71] This model is based on the adsorption capacity as a function of time and is given by the following equation (Eq. 11):

$$q_t = k_i\sqrt{t} + C \qquad (11)$$

with k_i refers to the intra-particle diffusion kinetic constant (mg g^{-1} $h^{-0.5}$) and C represents a conception about the thickness of the boundary layer.[72]

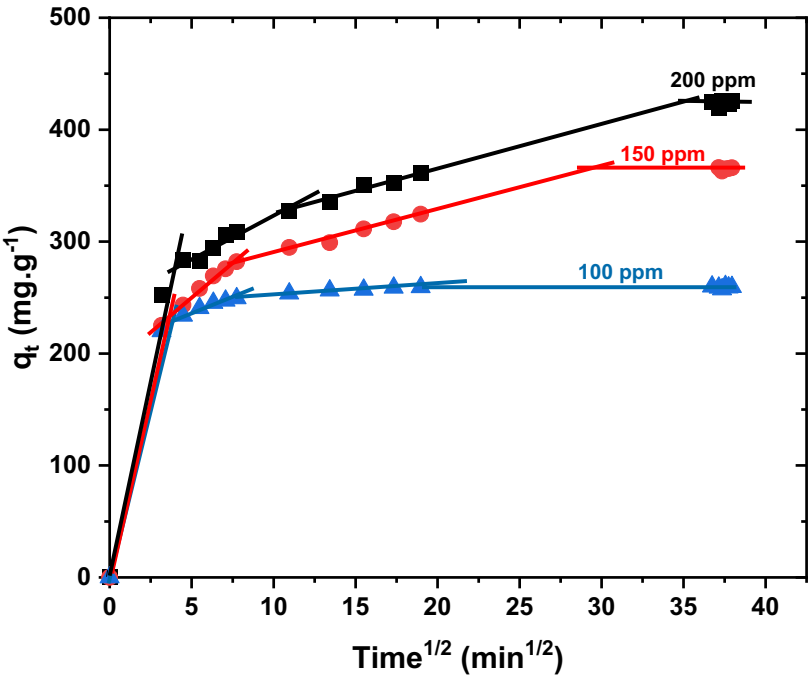

Figure 9. Intra-particle diffusion curves for TC adsorption in batch on CM (pH = 6, T = 298 K) with the Weber and Morris model (experimental data of Figure 8).

For the adsorption of TC on CM, the diffusion curves exhibit a multi-linearity relationship, suggesting that four stages may occur during the adsorption process (**Figure 9**). The first sharp stage stands for instantaneous external transfer; the diffusion of TC towards the external surface of CM, known as boundary layer diffusion, without intra-particle diffusion limitation during the first 5 h.[73] The second and third stages are two intra-particle diffusion phenomena, which represent the rate-limiting steps. The last stage is considered to be the final equilibrium in the adsorption process and depends on the amount of available adsorption sites within the material.[16] For the lower initial TC concentration (100 ppm), the slope of the second stage is small ($k_{id,2}$ = 3.8 mg g^{-1} $min^{-0.5}$), and the slopes of the third and fourth stages are very similar (**Table 5**), showing that for this amount of TC molecules, corresponding to an adsorption of 214 mg g^{-1}, there are almost no intra-particle diffusion limitations. We can anticipate that for initial TC concentration lower than 100 ppm, there will be no intra-particle diffusion limitations. In the literature, diffusion studies performed for TC adsorption on activated carbons usually

showed curves with three linear sections.[16-17] These activated carbons had a bimodal distribution of pores (micropores of 0.5-1 nm and supermicropores of 1.5-2 nm), with diffusion within the particles limited by the supermicropores. We can assume that the intra-particle diffusion stages found for CM are due to the two mesopore systems: the first intra-particle diffusion coefficient ($k_{id,2}$) could be controlled by diffusion through the small constricted mesopores and the second ($k_{id,3}$) by the larger mesopores (20-50 nm diameter).

Table 5. Intra-particle diffusion model constants and correlation coefficients for the adsorption of TC on CM

Parameters	**TC concentration**		
	100 ppm	150 ppm	200 ppm
$k_{id,1}$ (mg g^{-1} $min^{-0.5}$)	55.455	57.508	66.451
C_1 (mg g^{-1})	10.093	9.825	9.557
R^2	0.9452	0.9514	0.9651
$k_{id,2}$ (mg g^{-1} $min^{-0.5}$)	3.779	10.386	11.768
C_2 (mg g^{-1})	220.481	202.192	219.691
R^2	0.9724	0.9896	0.9694
$k_{id,3}$ (mg g^{-1} $min^{-0.5}$)	0.704	3.888	4.269
C_3 (mg g^{-1})	246.308	250.254	280.678
R^2	0.9639	0.9742	0.9694
$k_{id,4}$ (mg g^{-1} $min^{-0.5}$)	0.114	0.7897	0.204
C_4 (mg g^{-1})	255.068	335.404	417.438
R^2	0.7688	0.8783	0.8595

3.2.1.4 Effect of temperature for TC adsorption on CM

For an initial TC concentration of 100 mg L^{-1}, CM (375 mg L^{-1}) was able to adsorb 230 mg g^{-1} of TC after 24 h under stirring in batch at 298 K. Increasing the adsorption temperature from 288 to 308 K had no significant effect on the adsorption process (**Figure S12**). Identical kinetics and adsorption capacities have been reported in the literature for this TC concentration;[74-75] however, an increase in adsorption capacity has been observed at higher adsorption temperatures (323 K).[20]

3.2.2 Adsorption of TC on CM in flow

Very few studies address the adsorption of antibiotics under continuous flow. To the best of our knowledge, only breakthrough curves have been studied for TC adsorption[11,19,26] (**Table 6**). The efficient adsorption (Q_{eff}) was calculated with the time or the volume of solution passing through the column without any detectable molecule at the output of the column. Q_{eff} can be expressed as the mass of adsorbed molecules per gram of adsorbent (mg g^{-1}) or as the volume of solution efficiently treated per volume of adsorbent (L cm^{-3}), also named Volume by Bed Volume of adsorbent. The first detection of the molecule defines the breakthrough time (t_b). The total adsorption (Q_{total}) was calculated by integrating the breakthrough curve. In the literature, different initial concentrations (C_0) and flow rates (F) expressed as Darcy Rate (in m h^{-1}) (the flow rate in volume is divided by the section of the column) have been used. In the case of TC, there is often a small amount of non-adsorbed TC molecules coming out of the column since the beginning of adsorption, which concentration (C_b) remains constant until the breakthrough time (**Table 6**).

For CM used in continuous flow (**Figure S13**), the breakthrough curve also showed non-adsorbed TC molecules since the beginning (C_b/C_0 = 0.25) of the adsorption process, corresponding to a constant adsorption of 75% of TC molecules for 45 h before breakthrough. This phenomenon was certainly due to the preferential adsorption through electrostatic interaction of TC molecules containing the positively charged ammonium group (TCH^- and $TCH_2°$) on negatively charged CM and the repulsion of TC^{2-} molecules. Nevertheless, the adsorption capacity before breakthrough corresponds to an efficient adsorption in flow of 67 mg g^{-1} and a total adsorption of 110 mg g^{-1}, which are the highest values observed in the literature (**Table 6**). The high adsorption capacity of CM in continuous flow was certainly due to their highly porous network.

Merck's activated carbon (**Table S1**) resulted in almost complete adsorption of TC molecules prior to breakthrough (C_b/C_0 = 0.02)[11] (**Table 6**). A column of 1 cm diameter and 7 cm length showed a breakthrough curve with a highly efficient treatment of 2 L of TC solution at 20 ppm at a flow rate of 1.5 mL min^{-1} (1.14 m h^{-1}).[11] This corresponded to an efficient adsorption of 21 mg g^{-1} and a total adsorption of 60 mg g^{-1}. The adsorption capacities in continuous flow of both CM and Merck's activated carbon are inferior to their capacity in batch (~400 mg g^{-1}). To increase the adsorption capacity in flow, a new recirculation flow mode configuration was set up.

Table 6. Results of breakthrough curves for TC adsorption on CM in continuous flow. Comparison with the results of activated carbons in literature at different initial TC concentration (C_0) and flow rate (F): ratio of TC concentration at the beginning of the curve to initial concentration (C_b/C_0), time and adsorption capacity at breakthrough (t_b, Q_{eff}) and total capacity in flow (Q_{total}).

Carbon materials	L cm	F m h^{-1}	pH	C_0 ppm	C_b/C_0	t_b min	Q_{eff} mg g^{-1}	Q_{eff} L cm^{-3}	Q_{total} mg g^{-1}	Ref.
Bamboo	4	1.26	7	20	0.10	30	2	0.02	12	[19]
Apricot nut shell	4	18.4	5	20	0.05	55	14	0.42	50	[26]
Merck	7	1.14	4-5	20	0.02	1400	21	0.38	60	[11]
CM	3	1.08	9	10	0.25	2700	67	1.50	110	This work

In order to determine the maximum capacity of TC adsorption on CM under flow, a high concentrated solution of TC (200 ppm) was flowed for 24 h at a flow rate of 1 mL min^{-1} (**Figure S14**). This corresponded to an excess of 800 mg of TC per g of monolith. CM adsorbed 240 mg g^{-1} of TC in 5 h and 248 mg g^{-1} after 24 h. In batch, with infinite contact time, the maximum adsorption capacity was 420 mg g^{-1}, however 270 mg g^{-1} was adsorbed during the fast adsorption stage (within 1 h) (**Figures 8, 9**). This value agrees well with the maximum adsorption capacity found in flow (248 mg g^{-1}) for CM. The adsorption in flow (**Figure S14**) presents in fact two stages: a very fast adsorption within the first 30 min, corresponding to an adsorption of 133 mg g^{-1} and leading to a steady state during 3 h, and then an additional adsorption reaching the adsorption capacity of 240 mg g^{-1} after 5 h. This increase in adsorption after 3 h is likely due to either rearrangement of TC molecules on the surface of CM or diffusion of TC molecules into the mesopores, liberating spaces at the entrance of the mesopores to host further TC molecules. The very fast adsorption capacity of CM in flow is therefore 133 mg g^{-1} and their fast adsorption capacity is 240 mg g^{-1}. After this experiment, CM were recycled by flowing (1 mL min^{-1}) 80 mL of HCl (0.1 M) solution for 24 h. A second TC adsorption experiment was carried out and the same adsorption capacity (240 mg g^{-1}) was reached after 24 h. CM can therefore be recycled in situ and then used for further adsorption experiments. In recirculation flow mode, CM should decontaminate efficiently TC solutions with concentrations inferior to 60 ppm (corresponding to an adsorption of 240 mg g^{-1}) or inferior to

30 ppm (corresponding to an adsorption of 133 mg g^{-1}). The regeneration of CM could also be attempted with NaOH (0.1 or 0.2 M) solution, as previously reported in other studies with adsorption over nitrogen-doped carbon materials in batch.[56, 76]

3.3 Adsorption of a mixture of antibiotics on CM

3.3.1 Adsorption of a mixture of antibiotics on CM in batch

Very few examples of the adsorption of antibiotic mixture are reported in literature. A mixture of antibiotics (TC, chloramphenicol, ofloxacin, erythromycin) was performed in batch at very low concentration of antibiotics (0.1-1 mg L^{-1}) with a mesoporous N,P-doped carbon material prepared by hydrothermal pyrolysis with H_3PO_4 followed by a pyrolysis under N_2 at 500°C. The removal efficiency was greater than 97.5%.[56] However, no flow experiment was conducted. Prior to run the depollution of water contaminated with a mixture of antibiotics under flow with recirculation, the adsorption capacity of CM in batch was evaluated. In a solution containing ciprofloxacin (17.7 ppm), TC (21.6 ppm), amoxicillin (17.7 ppm) and sulfamethoxazole (17.5 ppm), 15 mg of grinded CM were added and stirred for 24 h (**Figure 10**). This corresponded to an amount of antibiotic of 815 mg g^{-1}. The initial pH of the solution in osmosed water was pH 6 and rose to pH 8 with the addition of CM. This is a more favorable pH for TC adsorption through electrostatic interactions with presumably COO^- functions of CM in this mixture of antibiotics as for a solution of TC alone. Indeed at pH 8, TC would appear as: $TCH_2°$ 33.3%, TCH^- 66.7% (100% of TC would feature the positively charged group $N^+(H)(CH_3)_2$)) (**Figure S10**).

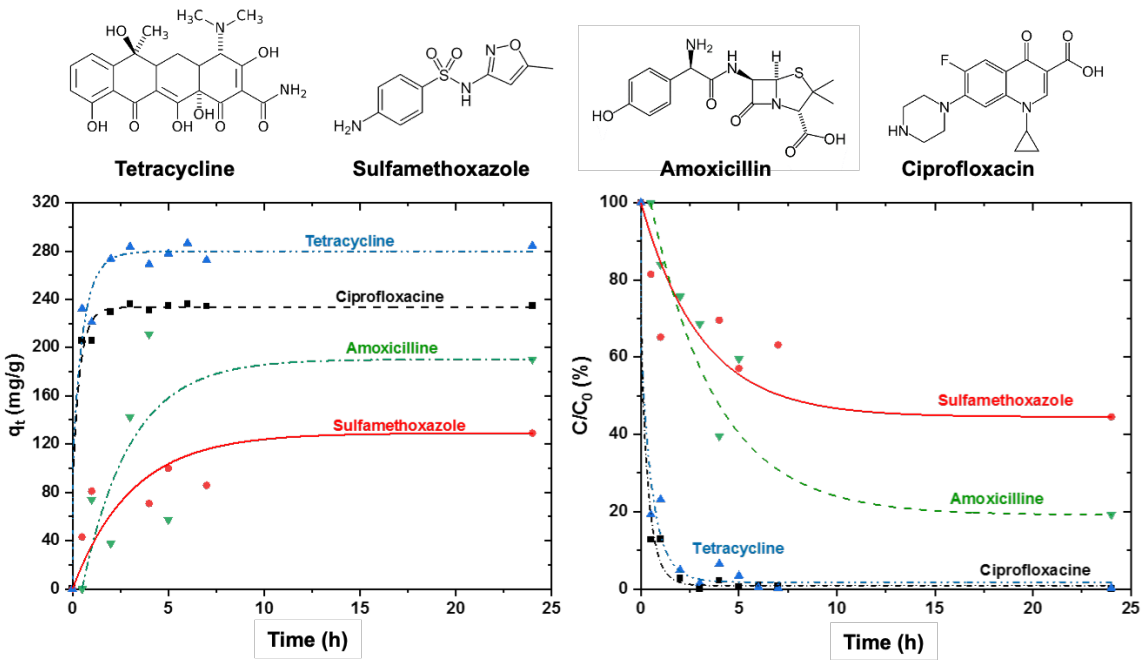

Figure 10. Adsorption of a mixture of pharmaceutical molecules (20 ppm each, 200 mL solution) with crushed CM (15 mg) in batch at 298 K under stirring (450 rpm). The lines are a guide for the eyes.

The adsorption of TC and ciprofloxacin in batch was very fast and reached almost 100% in 2 h. The adsorption of amoxicillin and sulfamethoxazole was slower and reached a steady state after 10 h.

The pH plays a critical role in the adsorption of antibiotics by carbon-based materials.[77] According to the pH, antibiotics would exist at different states, cationic, zwitterionic, neutral, anionic. The best pH for maximum removal of antibiotics is generally when they are under cationic forms leading to electrostatic interactions with negatively charged carbon-based materials. As our mixture of antibiotics with CM raises the pH of the solution to 8, it is therefore important to know the ionization state of the different antibiotics. Ciprofloxacin has pKa values of pka_1 = 5.9 and pKa_2 = 8.9.[78] At pH 8, the molecule is zwitterionic with functions NH_2^+ and COO^-. Electrostatic interactions between NH_2^+ groups of ciprofloxacin and COO^- groups of CM are possible. Electrostatic interactions between TC or ciprofloxacin might be responsible for the faster adsorption of these two molecules on CM in comparison to amoxicillin and sulfamethoxazole. Indeed, amoxicillin (pka_1 = 2.7, pKa_2 = 7.4, pKa_3 = 8.9)[79] and sulfamethoxazole (pKa_1 = 1.7, pKa_2 = 5.6)[80] are negatively charged at pH 8 and feature NH_2 and COO^- functionalities. No electrostatic interactions are possible with CM, which is negatively charged. However, H-bonding interactions between NH_2 groups of the molecules

and C=O groups of CM are possible, and maybe covalent bonds,[81] as well as π-π Electron-Donor-Acceptor (EDA) interactions, as proposed in literature[77,82] between the aromatic ring of sulfamethoxazole and amoxicillin and COO^- functions of CM. The adsorption capacity of CM for each molecule in batch was: 234 mg g^{-1} (0.70 mmol g^{-1}) for ciprofloxacin, 190 mg g^{-1} (0.52 mmol g^{-1}) for amoxicillin, 111 mg g^{-1} (0.44 mmol g^{-1}) for sulfamethoxazole and 280 mg g^{-1} (0.63 mmol g^{-1}) for TC, corresponding to 99, 80, 47, 97% removal efficiency, respectively. The total amount of antibiotics adsorbed is 2.29 mmol g^{-1}, 1.33 mmol g^{-1} by electrostatic interactions with COO^- groups of CM (TC and ciprofloxacin) and 0.96 mmol g^{-1} by H-bonding with C=O of CM or by π-π EDA interactions with COO^- groups of CM (sulfamethoxazole and amoxicillin). These values are compatible with the number of available functions of CM: 5.9 mmol g^{-1} COO^- and 1.5 mmol g^{-1} C=O (Table S1).

The total adsorption capacity for the mixture of pharmaceutical molecules in batch of CM was of 82%. It corresponded to 815 mg g^{-1} of pharmaceutical molecules adsorbed on CM. This result evidenced the outstanding potential capacity of CM as adsorbents for pharmaceutical molecules contained in waters.

The capacity of adsorption of CM in batch for the different pharmaceutical molecules was compared with the results reported in the literature, where activated carbons were predominantly reported as adsorbents but only for a single pharmaceutical molecule (**Table 7**). Therefore, the capacity of adsorption of CM obtained for each molecule in the mixture was compared with the adsorption of the single molecule on activated carbons. The adsorption of TC was already discussed and CM had a similar adsorption capacity as Merck's activated carbon (**Figure 7**). Merck's activated carbon featured an adsorption capacity for amoxicillin of 222-260 mg g^{-1},[13] which was slightly higher than for CM (190 mg g^{-1}). Similar adsorption capacity of ciprofloxacin was found for CM (234 mg g^{-1}) in comparison to another activated carbon (250 mg g^{-1}).[12] The adsorption capacity of CM was among the highest for sulfamethoxazole (111 mg g^{-1}) in comparison to most of activated carbons (58-95 mg g^{-1}) and comparable to graphene oxides (122 mg g^{-1}).[14] The presence of a large amount of carbonyl (C=O) and carboxylate (COO^-) groups in CM (Table S1) and the large volume of mesopores, which avoids steric hindrance, are favorable conditions for high adsorption capacity even at pH 8, in comparison to other activated carbons featuring only micropores and lower amount of functional groups. However, a commercial coal-based activated carbon from Norit, exhibits an adsorption capacity superior to the one of CM with an optimal value of 280 mg g^{-1}.[83] However,

the pH of the solution of sulfamethoxazole is not given in this work, and the adsorption capacity decreased drastically by a factor 2 going from pH 2 to pH 8 by the loss of electrostatic interactions.[83] Even if performed at pH 2, the values at pH 8 will remain higher than the capacity of CM. CM is among the best adsorbents to remove sulfamethoxazole. In batch, sulfamethoxazole was removed at 50%, corresponding to 111 mg/g, which seems to be the limit of adsorption for this molecule with CM.

Some studies showed that further post-treatment (HNO_3, NH_4Cl) of activated carbons followed by re-pyrolysis can increase the adsorption capacities of carbon materials.[12-13]

Table 7. Adsorption capacity of a mixture of pharmaceutical molecules (20 ppm each) contained in water of CM in batch and in flow. Comparison with literature data for single molecule adsorption in batch.

	Molecules mixture (20 ppm each)		Single molecule			
	CM Batch ($mg\ g^{-1}$)	CM Flow ($mg\ g^{-1}$)	CM Batch ($mg\ g^{-1}$)	Carbon NORIT ROX 0.8 [12] Batch ($mg\ g^{-1}$)	Carbons [14,83] Batch ($mg\ g^{-1}$)	Carbon Merck [13] Batch ($mg\ g^{-1}$)
ciprofloxacin	234	150		250[b]		
amoxicillin	190	150				222-260[d]
sulfamethoxazole	111	128			40-280[c]	
TC	280	140	420[a]			
Total	815	568				

[a] for literature comparison see Figure 7

[b] 330 mg/g if carbons are further treated with HNO_3 5 M at 130°C for 3 h followed by a pyrolysis under N_2 at 900°C.[12]

[c] 40-100 mg/g depending on the pH for most carbon-based materials[14] and 280 mg/g for a commercial coal-based activated carbon from Norit in batch and in flow (180 mg/g at breakthrough point).[83]

[d] 430 mg/g if carbons are further treated with NH_4Cl (2 wt%) 24 h followed by a pyrolysis under N_2 at 800°C for 2 h.[13]

3.3.2 Adsorption of a mixture of pharmaceutical molecules on CM in flow

The adsorption of the mixture of pharmaceutical molecules (~20 ppm each) was carried out in flow with a recirculation mode at a flow rate of 1 mL min^{-1} (**Figure 11, Figure S15**). TC and sulfamethoxazole were preferentially adsorbed on CM. The adsorption of TC and sulfamethoxazole on CM was very fast with almost 90% of adsorption in 5 h and reached 97 and 100% after 24 h, respectively. The adsorption of amoxicillin and ciprofloxacin on CM was slower. After 24 h, amoxicillin was adsorbed at 91% and ciprofloxacin at 85%. The initial rate of adsorption of TC and ciprofloxacin was similar for both molecules but the rate of adsorption decreases for ciprofloxacin after 2 h (**Figure S15**). TC and ciprofloxacin molecules are in competition for COO^- sites of adsorption of CM and TC has therefore preferential electrostatic interactions with COO^-. The initial rate of adsorption of sulfamethoxazole is higher than the one of amoxicillin for both molecules in H-bonding between their NH_2 groups and C=O groups of CM or in π-π EDA interactions between their benzene ring and COO^- groups of CM. Nevertheless, the initial rate of adsorption of sulfamethoxazole TC are similar. Indeed, both molecules do not seem in competition for COO^- sites of adsorption. We can then assume that sulfamethoxazole interacts mainly by H-bonding with C=O groups of CM and consider that this interaction is stronger than the H-bonding with amoxicillin. The high rate of adsorption in flow of sulfamethoxazole could be also due to the relative small size of this molecule, leading to a faster diffusion towards the C=O active sites of CM in comparison to amoxicillin.

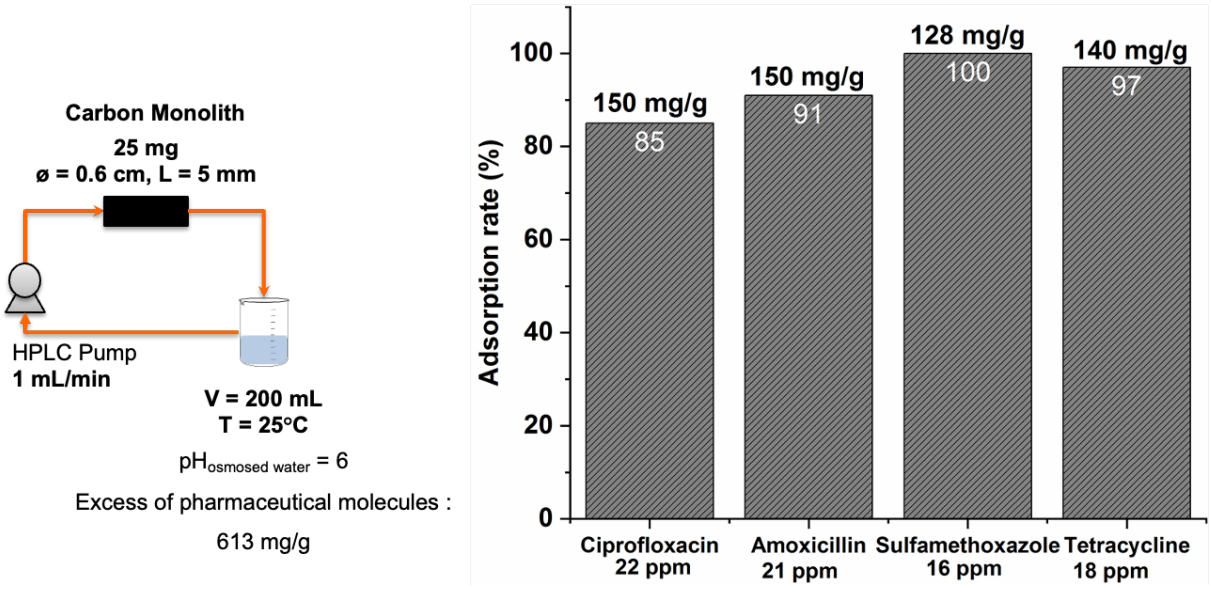

Figure 11. (left) Schematic representation of the experimental set-up. (right) Adsorption rate (%) and adsorption capacity (mg g^{-1}) of pharmaceutical micropollutants (20 ppm each) on CM

at a flow rate of 1 mL min^{-1} after 24 h in a recirculation flow mode at 298 K. The precise initial concentration for each pharmaceutical molecule is measured by HPLC-MS.

The adsorption capacity in flow of the different pharmaceutical molecules on CM was after 24 h: 150 mg g^{-1} for ciprofloxacin (0.45 mmol g^{-1}), 150 mg g^{-1} for amoxicillin (0.41 mmol g^{-1}), 128 mg g^{-1} (0.50 mmol g^{-1}) for sulfamethoxazole and 140 mg g^{-1} (0.31 mmol g^{-1}) for tetracycline (**Table 7**), which corresponded to 85, 91, 100 and 97% of adsorption of the molecules, respectively (**Figure 11**). A total of 568 mg g^{-1} (1.68 mmol g^{-1}) was adsorbed on CM in flow, corresponding to a removal capacity of pharmaceutical molecules of 93%. This process of water decontamination by adsorption was more efficient than the process of depollution by biocatalysis previously developed with enzymes (laccases) grafted on silica monoliths under similar conditions.[42] The elimination efficiency after 24 h was 100% for amoxicillin, 60% for sulfamethoxazole, 55% for tetracycline and 30% for ciprofloxacin, corresponding to a total removal capacity for pharmaceutical molecules of 64%. CM are certainly an efficient solution for the depollution of waters contaminated with pharmaceutical molecules under flow conditions. Furthermore, this process is safer and easier to develop compared to packed-bed processes, since no particles need to be manipulated.

Before conclusions can be drawn about CM efficiency, further studies should be performed to analyze their behavior in the presence of salts, natural organic matter (NOM) and microorganisms as in real wastewaters.[11,77,82,84] Mineral water contains Na^+, K^+, Mg^{2+}, Ca^{2+} cations in the range of concentrations 0.2, 0.02, 1, 2 mM, respectively. Indeed, in the literature it has been reported that the ionic strength of the solution could affect the adsorption capacity of CM.[77, 84] In the case of graphene oxide (GO), authors[82] show that salts have low effect on antibiotics adsorption if the mechanism is not governed by electrostatic interactions as in the case of sulfamethoxazole. The results clearly showed that $CaCl_2$ (0.3 and 3.0 mM) had no influence on the adsorption of sulfamethoxazole, while high NaCl concentration (20 and 200 mM) slightly reduced the adsorption of sulfamethoxazole (from 55 to 32-38 mg g^{-1}). In the case of major electrostatic interactions between antibiotics and GO, like for ciprofloxacin, the adsorption capacity decreased by half with $CaCl_2$ (0.3 and 3.0 mM) from 140 to 85 and 75 mg g^{-1}, respectively, as Ca^{2+} complex the carboxyl groups of GO. NaCl only influenced the adsorption at high ionic strength (200 mM). It is also the case for TC adsorbed on petroleum coke activated carbon, where the addition of salts in concentration 10 - 100 mM, showed no influence of NaCl and KCl, a little influence $MgCl_2$, and a little influence of $CaCl_2$ at 10 mM, but a strong influence of $CaCl_2$ at 100 mM with the adsorption reduced by 60%.[16] The presence

of NOM, such as humic acid and fulvic acid, has been scarcely investigated for the adsorption of antibiotics on carbon-based materials.[77] NOM are supposed to reduce adsorption through pore blocking and competitive adsorption. However, in the case of CM, we can hypothesize that large mesopores would avoid pore blocking, and the pH of 8 induced by CM would induce repulsive interaction with carboxylic acids as NOM.

4. Conclusions

The CM synthesized in this work by replicating silica monoliths exhibit hierarchical micro-/meso-/macroporosity, high surface area (1058 m^2/g), high pore volume (6.8 mL/g) and excellent permeability (3.55 10^{-12} m^2) due to a homogeneous network of interconnected macropores. They feature excellent properties to be used as adsorbents in a continuous flow for water purification. Their surface chemistry differs from that of activated carbons because they are basic and negatively charged. CM were first tested as adsorbents with a single pharmaceutical molecule, tetracycline (TC). Batch adsorption of TC showed that the adsorption isotherm was consistent with the Temkin model and that the adsorption kinetics followed a pseudo-second order model. This indicates that: (i) CM have heterogeneous adsorption sites, (ii) the heat of adsorption decreases with surface coverage, (iii) adsorption occurs through electrostatic interactions between the negative charges of CM and the positively charged ammonium groups of TC. The maximum adsorption capacity of TC in batch was 420 mg g^{-1}. The diffusion study reveals a fast capacity of adsorption in batch of 270 mg g^{-1} without diffusion limitations. The maximum adsorption capacity in flow-through, realized with a recirculation mode, was 133 mg g^{-1} in 1 h and 250 mg g^{-1} in 24 h. The adsorption of TC (10 ppm) under continuous flow showed a breakthrough curve with a constant adsorption of 75% of TC for 45 h, mainly due to the repulsion of the negatively charged TC molecules at the pH of the solution (pH 9). The efficient adsorption capacity was 67 mg g^{-1} and the total adsorption was 110 mg g^{-1}. Flow-through adsorption in recirculation mode should be preferred to ensure higher adsorption capacity. CM were further used as adsorbents for waters containing a mixture of pharmaceutical molecules (20 ppm each). The adsorption capacity of CM after 24 hours in batch for each molecule was: 234 mg g^{-1} for ciprofloxacin, 190 mg g^{-1} for amoxicillin, 111 mg g^{-1} for sulfamethoxazole and 280 mg g^{-1} for TC, corresponding to 99, 80, 47, and 97% elimination by adsorption, respectively. The total adsorption capacity in batch was 82% and corresponded to 815 mg g^{-1} of pharmaceutical molecules adsorbed on CM. The higher adsorption capacity of TC was due to a lower pH of the solution (pH 8) due to the presence of

the other pharmaceutical molecules. At this pH all TC molecules possess the positively charged ammonium group. The adsorption capacity in flow in recirculation mode of the different pharmaceutical molecules on CM after 24 hours was: 150 mg g^{-1} for ciprofloxacin, 150 mg g^{-1} amoxicilin, 128 mg g^{-1} for sulfamethoxazole and 140 mg g^{-1} tetracycline, which corresponded to adsorption of 85, 91, 100 and 97% of the molecules, respectively. A total of 568 mg g^{-1} was adsorbed on CM, which corresponded to a removal capacity of 93% of the pharmaceutical molecules.

CM proved to be excellent adsorbents for mixtures of pharmaceutical molecules contained in water under both batch and flow-through conditions. The concentrations of pharmaceutical molecules used in this study for analytic purpose (20 mg L^{-1}) are much higher than in real wastewater (ng-µg L^{-1}) and we can emphasize that CM would be excellent candidates for the purification of real wastewater contaminated by pharmaceutical molecules.

Acknowledgements

This work was supported by the ANR French agency, project MUSE ANR-16-IDEX-0006 DEMEMO. The authors wish to acknowledge the support of the plateform MEA (University of Montpellier), where SEM and TEM have been performed. NB would like to thank Clément Sanchez for his inspiring work and support in the early years of his academic career.

Supporting Information

- Micro-CT analysis of CM and silica monolith
- Pore size distribution of CM using SAIEUS software with the carbon 2D-NLDFT heterogeneous surface model applied to the N_2 sorption isotherm at 77 K
- Zeta potential of CM
- XPS of CM
- TGA of CM compared to the parent silica monolith
- TC structure and speciation diagram as a function of pH
- Langmuir, Freundlich and Temkin models fitting for the adsorption of TC on CM
- Breakthrough curve of TC adsorption with CM in continuous flow without recirculation
- Adsorption of TC on CM in continuous flow with recirculation
- Adsorption of pharmaceutical micropollutants in CM as a function of time in continuous flow with recirculation
- Comparison of CM with Merck's activated carbon

References

1. Stumm-Zollinger, E.; Fair, G. M., Biodegradation of Steroid Hormones. *J. Water Pollut. Control Fed.* **1965,** *37* (11), 1506-1510.
2. Norpoth, K.; Nehrkorn, A.; Kirchner, M.; Holsen, H.; Teipel, H., Studies on the problem of solubility and stability of steroid ovulation inhibitors in water, waste water and activated sludge. *Zentralbl. Bakteriol. Orig. B* **1973,** *156* (6), 500-511.
3. Larsson, D. G. J.; Adolfsson-Erici, M.; Parkkonen, J.; Pettersson, M.; Berg, A. H.; Olsson, P. E.; Förlin, L., Ethinyloestradiol — an undesired fish contraceptive? *Aquat. Toxicol.* **1999,** *45* (2), 91-97.
4. Oaks, J. L.; Gilbert, M.; Virani, M. Z.; Watson, R. T.; Meteyer, C. U.; Rideout, B. A.; Shivaprasad, H. L.; Ahmed, S.; Iqbal Chaudhry, M. J.; Arshad, M.; Mahmood, S.; Ali, A.; Ahmed Khan, A., Diclofenac residues as the cause of vulture population decline in Pakistan. *Nature* **2004,** *427* (6975), 630-633.
5. Chen, M.-Y.; Ike, M.; Fujita, M., Acute toxicity, mutagenicity, and estrogenicity of bisphenol-A and other bisphenols. *Environ. Toxicol.* **2002,** *17* (1), 80-86.
6. Ling, A. L.; Pace, N. R.; Hernandez, M. T.; LaPara, T. M., Tetracycline resistance and class 1 integron genes associated with indoor and outdoor aerosols. *Environ. Sci. Technol.* **2013,** *47* (9), 4046-4052.
7. Agency, E. M., Sales of veterinary antimicrobial agents in 31 european countries in 2019 and 2020, Trends from 2010 to 2020. *Eleventh ESVAC report* **2021**, 130.
8. Watkinson, A.; Murby, E.; Kolpin, D. W.; Costanzo, S., The occurrence of antibiotics in an urban watershed: from wastewater to drinking water. *Sci. Total Environ.* **2009,** *407* (8), 2711-2723.
9. Wang, Z.; Chen, Q.; Zhang, J.; Dong, J.; Yan, H.; Chen, C.; Feng, R., Characterization and source identification of tetracycline antibiotics in the drinking water sources of the lower Yangtze River. *J. Environ. Manage.* **2019,** *244*, 13-22.
10. Zang, J.; Wu, T.; Song, H.; Zhou, N.; Fan, S.; Xie, Z.; Tang, J., Removal of Tetracycline by Hydrous Ferric Oxide: Adsorption Kinetics, Isotherms, and Mechanism. *Int. J. Environ. Res. Public Health* **2019,** *16* (22), 4580.
11. Rivera-Utrilla, J.; Gómez-Pacheco, C. V.; Sánchez-Polo, M.; López-Peñalver, J. J.; Ocampo-Pérez, R., Tetracycline removal from water by adsorption/bioadsorption on activated carbons and sludge-derived adsorbents. *J. Environ. Manage.* **2013,** *131*, 16-24.
12. Carabineiro, S. A. C.; Thavorn-Amornsri, T.; Pereira, M. F. R.; Figueiredo, J. L., Adsorption of ciprofloxacin on surface-modified carbon materials. *Water Res.* **2011,** *45* (15), 4583-4591.
13. Moussavi, G.; Alahabadi, A.; Yaghmaeian, K.; Eskandari, M., Preparation, characterization and adsorption potential of the NH_4Cl-induced activated carbon for the removal of amoxicillin antibiotic from water. *Chem. Eng. J.l* **2013,** *217*, 119-128.
14. Pamphile, N.; Xuejiao, L.; Guangwei, Y.; Yin, W., Synthesis of a novel core-shell-structure activated carbon material and its application in sulfamethoxazole adsorption. *J. Hazard. Mater.* **2019,** *368*, 602-612.
15. Zhang, L.; Song, X.; Liu, X.; Yang, L.; Pan, F.; Lv, J., Studies on the removal of tetracycline by multi-walled carbon nanotubes. *Chem. Eng. J.* **2011,** *178*, 26-33.
16. Zhang, D.; Yin, J.; Zhao, J.; Zhu, H.; Wang, C., Adsorption and removal of tetracycline from water by petroleum coke-derived highly porous activated carbon. *J. Environ. Chem. Eng.* **2015,** *3* (3), 1504-1512.

17. Martins, A. C.; Pezoti, O.; Cazetta, A. L.; Bedin, K. C.; Yamazaki, D. A. S.; Bandoch, G. F. G.; Asefa, T.; Visentainer, J. V.; Almeida, V. C., Removal of tetracycline by NaOH-activated carbon produced from macadamia nut shells: Kinetic and equilibrium studies. *Chem.l Eng. J.* **2015,** *260*, 291-299.
18. Liu, P.; Liu, W.-J.; Jiang, H.; Chen, J.-J.; Li, W.-W.; Yu, H.-Q., Modification of bio-char derived from fast pyrolysis of biomass and its application in removal of tetracycline from aqueous solution. *Bioresour. Technol.* **2012,** *121*, 235-240.
19. Liao, P.; Zhan, Z.; Dai, J.; Wu, X.; Zhang, W.; Wang, K.; Yuan, S., Adsorption of tetracycline and chloramphenicol in aqueous solutions by bamboo charcoal: a batch and fixed-bed column study. *Chem. Eng. J.l* **2013,** *228*, 496-505.
20. Chen, J.; Fei, Z.; Tao, W.; Zhang, G., Adsorption and desorption of tetracycline on activated carbons, *Advanced Materials Research*, *Trans Tech Publ*., **2011**, *233-235*, 561-566.
21. Wu, K.; Zhang, C.; Liu, T.; Lei, H.; Yang, S.; Jin, P., The removal of tetracycline, oxytetracycline, and chlortetracycline by manganese oxide–doped copper oxide: the behaviors and insights of Cu-Mn combination for enhancing antibiotics removal. *Environ. Sci. Pollut. Res.* **2020,** *27* (11), 12613-12623.
22. Pi, S.; Li, A.; Wei, W.; Feng, L.; Zhang, G.; Chen, T.; Zhou, X.; Sun, H.; Ma, F., Synthesis of a novel magnetic nano-scale biosorbent using extracellular polymeric substances from Klebsiella sp. J1 for tetracycline adsorption. *Bioresour. Technol.* **2017,** *245*, 471-476.
23. Sánchez-Polo, M.; Velo-Gala, I.; López-Peñalver, J. J.; Rivera-Utrilla, J., Molecular imprinted polymer to remove tetracycline from aqueous solutions. *Microporous Mesoporous Mater.* **2015,** *203*, 32-40.
24. Long, R. Q.; Yang, R. T., Carbon nanotubes as superior sorbent for dioxin removal. *J. Amer. Chem. Soc.* **2001,** *123* (9), 2058-2059.
25. Chen, J.; Chen, W.; Zhu, D., Adsorption of nonionic aromatic compounds to single-walled carbon nanotubes: effects of aqueous solution chemistry. *Environ. Sci. Technol.* **2008,** *42* (19), 7225-7230.
26. Marzbali, M. H.; Esmaieli, M., Fixed bed adsorption of tetracycline on a mesoporous activated carbon: Experimental study and neuro-fuzzy modeling. *J. Appl. Res. Technol.* **2017,** *15* (5), 454-463.
27. Ocampo-Pérez, R.; Rivera-Utrilla, J.; Gómez-Pacheco, C.; Sánchez-Polo, M.; López-Peñalver, J., Kinetic study of tetracycline adsorption on sludge-derived adsorbents in aqueous phase. *Chem. Eng. J.* **2012,** *213*, 88-96.
28. Baccour, M.; Lamotte, A.; Sakai, K.; Dubreucq, E.; Mehdi, A.; Kano, K.; Galarneau, A.; Drone, J.; Brun, N., Production of formate from CO_2 gas under ambient conditions: towards flow-through enzyme reactors. *Green Chem.* **2020,** *22* (12), 3727-3733.
29. Yu, L.; Brun, N.; Sakaushi, K.; Eckert, J.; Titirici, M. M., Hydrothermal nanocasting: Synthesis of hierarchically porous carbon monoliths and their application in lithium–sulfur batteries. *Carbon* **2013,** *61*, 245-253.
30. Galarneau, A.; Sachse, A.; Said, B.; Pelisson, C.-H.; Boscaro, P.; Brun, N.; Courtheoux, L.; Olivi-Tran, N.; Coasne, B.; Fajula, F., Hierarchical porous silica monoliths: A novel class of microreactors for process intensification in catalysis and adsorption. *C. R. Chimie* **2016,** *19* (1-2), 231-247.
31. Galarneau, A.; Abid, Z.; Said, B.; Didi, Y.; Szymanska, K.; Jarzębski, A.; Tancret, F.; Hamaizi, H.; Bengueddach, A.; Di Renzo, F., Synthesis and textural characterization of mesoporous and meso-/macroporous silica monoliths obtained by spinodal decomposition. *Inorganics* **2016,** *4* (2), 9.
32. Lu, X.; Nakanishi, K., Synthesis of Hierarchically Porous Metal Oxide Monoliths via Sol–Gel Process Accompanied by Phase Separation From Divalent Metal Salts: A Short Review. *Front. Chem. Eng.* **2021,** *3*.

33. Puy, G.; Roux, R.; Demesmay, C.; Rocca, J.-L.; Iapichella, J.; Galarneau, A.; Brunel, D., Influence of the hydrothermal treatment on the chromatographic properties of monolithic silica capillaries for nano-liquid chromatography or capillary electrochromatography. *J. Chrom. A* **2007,** *1160* (1-2), 150-159.
34. Puy, G.; Demesmay, C.; Rocca, J. L.; Iapichella, J.; Galarneau, A.; Brunel, D., Electrochromatographic behavior of silica monolithic capillaries of different skeleton sizes synthesized with a simplified and shortened sol–gel procedure. *Electrophoresis* **2006,** *27* (20), 3971-3980.
35. El Kadib, A.; Chimenton, R.; Sachse, A.; Fajula, F.; Galarneau, A.; Coq, B., Functionalized Inorganic Monolithic Microreactors for High Productivity in Fine Chemicals Catalytic Synthesis. *Angew. Chem., Intern. Ed.* **2009,** *48* (27), 4969-4972.
36. Sachse, A.; Hulea, V.; Finiels, A.; Coq, B.; Fajula, F.; Galarneau, A., Alumina-grafted macro-/mesoporous silica monoliths as continuous flow microreactors for the Diels–Alder reaction. *J. Catal.* **2012,** *287*, 62-67.
37. Sachse, A.; Ameloot, R.; Coq, B.; Fajula, F.; Coasne, B.; De Vos, D.; Galarneau, A., In situ synthesis of Cu–BTC (HKUST-1) in macro-/mesoporous silica monoliths for continuous flow catalysis. *Chem. Comm.* **2012,** *48* (39), 4749-4751.
38. Sachse, A.; Linares, N.; Barbaro, P.; Fajula, F.; Galarneau, A., Selective hydrogenation over Pd nanoparticles supported on a pore-flow-through silica monolith microreactor with hierarchical porosity. *Dalton Trans.* **2013,** *42* (5), 1378-1384.
39. Linares, N.; Hartmann, S.; Galarneau, A.; Barbaro, P., Continuous Partial Hydrogenation Reactions by Pd@unconventional Bimodal Porous Titania Monolith Catalysts. *ACS Catal.* **2012,** *2* (10), 2194-2198.
40. Jatoi, H. U. K.; Goepel, M.; Poppitz, D.; Kohns, R.; Enke, D.; Hartmann, M.; Gläser, R., Mass Transfer in Hierarchical Silica Monoliths Loaded With Pt in the Continuous-Flow Liquid-Phase Hydrogenation of p-Nitrophenol. *Front. Chem. Eng.* **2021,** *3*.
41. Szymańska, K.; Ciemięga, A.; Maresz, K.; Pudło, W.; Malinowski, J.; Mrowiec-Białoń, J.; Jarzębski, A. B., Catalytic Functionalized Structured Monolithic Micro-/Mesoreactors: Engineering, Properties, and Performance in Flow Synthesis: An Overview and Guidelines. *Front. Chem. Eng.* **2021,** *3*.
42. Sebai, W.; Ahmad, S.; Belleville, M.-P.; Boccheciampe, A.; Chaurand, P.; Levard, C.; Brun, N.; Galarneau, A.; Sanchez-Marcano, J., Biocatalytic Elimination of Pharmaceutics Found in Water With Hierarchical Silica Monoliths in Continuous Flow. *Front. Chem. Eng.* **2022,** *4*.
43. Forte, P.; Sachse, A.; Maes, M.; Galarneau, A.; De Vos, D., Selective continuous flow extractive denitrogenation of oil containing S- and N-heteroaromatics using metal-containing ionic liquids supported on monolithic silica with hierarchical porosity. *RSC Adv.* **2014,** *4* (3), 1045-1054.
44. Said, B.; Grandjean, A.; Barré, Y.; Tancret, F.; Fajula, F.; Galarneau, A., LTA zeolite monoliths with hierarchical trimodal porosity as highly efficient microreactors for strontium capture in continuous flow. *Microporous Mesoporous Mater.* **2016,** *232*, 39-52.
45. Didi, Y.; Said, B.; Micolle, M.; Cacciaguerra, T.; Cot, D.; Geneste, A.; Fajula, F.; Galarneau, A., Nanocrystals FAU-X monoliths as highly efficient microreactors for cesium capture in continuous flow. *Microporous Mesoporous Mater.* **2019,** *285*, 185-194.
46. Ahmad, S.; Sebai, W.; Belleville, M. P.; Brun, N.; Galarneau, A.; Sanchez-Marcano, J., Enzymatic monolithic reactors for micropollutants degradation. *Catal. Today* **2021,** *362*, 62-71.
47. Rouquerol, J.; Llewellyn, P.; Rouquerol, F., Is the BET equation applicable to microporous adsorbents? In *Characterization of Porous Solids VII - Proceedings of the 7th International Symposium on the Characterization of Porous Solids (COPS-VII), Aix-en-Provence, France, 26-28 May 2005*, 2007; pp 49-56.

48. Galarneau, A.; Mehlhorn, D.; Guenneau, F.; Coasne, B.; Villemot, F.; Minoux, D.; Aquino, C.; Dath, J.-P., Specific surface area determination for microporous/mesoporous materials: The case of mesoporous FAU-Y zeolites. *Langmuir* **2018,** *34* (47), 14134-14142.
49. Broekhoff, J. C. P.; de Boer, J. H., Studies on pore systems in catalysts: XIV. Calculation of the cumulative distribution functions for slit-shaped pores from the desorption branch of a nitrogen sorption isotherm. *J. Catal.* **1968,** *10* (4), 391-400.
50. Galarneau, A.; Desplantier, D.; Dutartre, R.; Di Renzo, F., Micelle-templated silicates as a test bed for methods of mesopore size evaluation. *Microporous Mesoporous Mater.* **1999,** *27* (2-3), 297-308.
51. Groen, J. C.; Peffer, L. A. A.; Pérez-Ramírez, J., Incorporation of appropriate contact angles in textural characterization by mercury porosimetry. *Stud. Surf. Sci. Catal.* **2002,** *144*, 91-98.
52. Ikeda, S.; Tachi, K.; Ng, Y. N.; Ikoma, Y.; Sakata, T.; Mori, H.; Harada, T.; Matsumura, M., Selective Adsorption of Glucose-Derived Carbon Precursor on Amino-Functionalized Porous Silica for Fabrication of Hollow Carbon Spheres with Porous Walls. *Chem. Mater.* **2007,** *19*, 4335-4340.
53. Galarneau, A.; Lefèvre, B.; Cambon, H.; Coasne, B.; Valange, S.; Gabelica, Z.; Bellat, J.-P.; Di Renzo, F., Pore-Shape Effects in Determination of Pore Size of Ordered Mesoporous Silicas by Mercury Intrusion. *J. Phys. Chem. C* **2008,** *112*, 12921-12927.
54. Coasne, B.; Galarneau, A.; Di Renzo, F.; Pellenq, R. J. M., Intrusion and Retraction of Fluids in Nanopores: Effect of Morphological Heterogeneity. *J. Phys. Chem. C* **2009,** *113*, 1953-1962.
55. Coasne, B.; Galarneau, A.; Di Renzo, F.; Pellenq, R. J. M., Effect of morphological defect on gas adsorption in nanoporous silicas. *J. Phys. Chem. C* **2007,** *111*, 15759-15770.
56. Huang, K.; Yang, S.; Liu, X.; Zhu, C.; Qi, F.; Wang, K.; Wang, J.; Wang, Q.; Wang, T.; Ma, P., Adsorption of antibiotics from wastewater by cabbage-based N, P co-doped mesoporous carbon materials. *J. Clean. Prod.* **2023,** *391*, 136174.
57. Panda, M. N.; Lake, L. W., Estimation of Single-Phase Permeability from Parameters of Particle-Size Distribution. *AAPG Bulletin* **1994,** *78* (7), 1028 - 1039.
58. Mojica, E.-R. E.; Nguyen, E.; Rozov, M.; Bright, F. V., pH-dependent spectroscopy of tetracycline and its analogs. *J. Fluoresc.* **2014,** *24* (4), 1183-1198.
59. Giles, C. H.; Smith, D.; Huitson, A., A general treatment and classification of the solute adsorption isotherm. I. Theoretical. *J. Colloid Interf. Sci.* **1974,** *47* (3), 755-765.
60. Langmuir, I., The adsorption of gases on plane surfaces of glass, mica and platinum. *J. Amer. Chem. Soc.* **1918,** *40* (9), 1361-1403.
61. Freundlich, H., *The Elements of Colloidal Chemistry*. EP Dutton and Company: 1924.
62. Temkin, M. I., Kinetics of ammonia synthesis on promoted iron catalysts. *Acta Physiochim. URSS* **1940,** *12*, 327-356.
63. Hadi, M.; Samarghandi, M. R.; McKay, G., Equilibrium two-parameter isotherms of acid dyes sorption by activated carbons: study of residual errors. *Chem. Eng. J.* **2010,** *160* (2), 408-416.
64. Tan, I.; Ahmad, A.; Hameed, B., Adsorption isotherms, kinetics, thermodynamics and desorption studies of 2, 4, 6-trichlorophenol on oil palm empty fruit bunch-based activated carbon. *J. Hazard. Mater.* **2009,** *164* (2-3), 473-482.
65. Pezoti Jr, O.; Cazetta, A. L.; Souza, I. P.; Bedin, K. C.; Martins, A. C.; Silva, T. L.; Almeida, V. C., Adsorption studies of methylene blue onto ZnCl2-activated carbon produced from buriti shells (Mauritia flexuosa L.). *J. Ind. Eng. Chem.* **2014,** *20* (6), 4401-4407.
66. Jang, H. M.; Yoo, S.; Choi, Y.-K.; Park, S.; Kan, E., Adsorption isotherm, kinetic modeling and mechanism of tetracycline on Pinus taeda-derived activated biochar. *Bioresour. Technol.* **2018,** *259*, 24-31.

67. Benyahia, F.; O'Neill, K. E., Enhanced voidage correlations for packed beds of various particle shapes and sizes. *Part. Sci. Technol.* **2005,** *23* (2), 169-177.
68. Reich, S.-J.; Svidrytski, A.; Hlushkou, D.; Stoeckel, D.; Kübel, C.; Höltzel, A.; Tallarek, U., Hindrance factor expression for diffusion in random mesoporous adsorbents obtained from pore-scale simulations in physical reconstructions. *Ind. Eng. Chem. Res.* **2018,** *57* (8), 3031-3042.
69. Lagergren, S., Zur theorie der sogenannten adsorption geloster stoffe, *Kungliga Svenska Vetenskapsakademiens. Handlinga*r, **1898**, 24 (4), 1-39.
70. Ho, Y.-S.; McKay, G., Pseudo-second order model for sorption processes. *Process Biochem.* **1999,** *34* (5), 451-465.
71. Weber Jr, W., JCM. Kinetics of Adsorption on Carbon from Solution. *J. Sanit. Eng.* **1963,** *504*, 89.
72. Crini, G.; Peindy, H. N.; Gimbert, F.; Robert, C., Removal of C.I. Basic Green 4 (Malachite Green) from aqueous solutions by adsorption using cyclodextrin-based adsorbent: Kinetic and equilibrium studies. *Sep. Purif. Technol.* **2007,** *53* (1), 97-110.
73. Hameed, B.; Tan, I.; Ahmad, A., Adsorption isotherm, kinetic modeling and mechanism of 2, 4, 6-trichlorophenol on coconut husk-based activated carbon. *Chem. Eng. J.* **2008,** *144* (2), 235-244.
74. Gao, Y.; Li, Y.; Zhang, L.; Huang, H.; Hu, J.; Shah, S. M.; Su, X., Adsorption and removal of tetracycline antibiotics from aqueous solution by graphene oxide. *J. Colloid Interf. Sci.* **2012,** *368* (1), 540-546.
75. Huang, L.; Wang, M.; Shi, C.; Huang, J.; Zhang, B., Adsorption of tetracycline and ciprofloxacin on activated carbon prepared from lignin with H_3PO_4 activation. *Desalination Water Treat.* **2014,** *52* (13-15), 2678-2687.
76. Peng, X.; Luo, Z.; Xie, H.; Liang, W.; Luo, J.; Dang, C.; Wang, A.; Hu, L.; YU, X.; Cai, W., Removal of phenylarsonic acid compounds by porous nitrogen doped carbon: Experimental and DFT study. *Appl. Surf. Sci.* **2022,** *606*, 154859.
77. Xiang, Y.; Xu, Z.; Wei, Y.; Zhou, Y.; Yang, X.; Yang, Y.; Yang, J.; Zhang, J.; Luo, L.; Zhou, Z., Carbon-based materials as adsorbent for antibiotics removal: Mechanisms and influencing factors. *J. Environ. Manage.* **2019,** *237*, 128-138.
78. Igwegbe, C. A.; Oba, S. N.; Aniagor, C. O.; Adeniyi, A. G.; Ighalo, J. O., Adsorption of ciprofloxacin from water: A comprehensive review. *J. Ind. Eng. Chem.* **2021,** *93*, 57-77.
79. Sallam, S.; Alorabi, A. Q.; Almotairy, A. R. Z.; Ibarhiam, S. F.; Aljuhani, E.; Al-Qahtani, S. D.; El-Metwaly, N. M., Superior and effective adsorption of amoxicillin by using novel metal organic framework and its composite: Thermodynamic, kinetic, and optimization by Box–Behnken design. *Appl. Organomet. Chem.* **2023,** *37*, e7184.
80. Nghiem, L. D.; Schäfer, A. I.; Elimelech, M., Pharmaceutical Retention Mechanisms by Nanofiltration Membranes. *Environ. Sci. Technol.* **2005,** *39*, 7698-7705.
81. Wu, J.; Wang, R.; Zhang, Y.; Chen, B.; Zhu, X. In situ scrutinize the adsorption of sulfamethoxazole in water using AFM force spectroscopy: Molecular adhesion force determination and fractionation. *J. Hazard. Mater.* **2022**, 426, 128128.
82. Chen, H.; Gao, B.; Li, H., Removal of sulfamethoxazole and ciprofloxacin from aqueous solutions by graphene oxide. *J. Hazard. Mater.* **2015,** *282*, 201-207.
83. Çalışkan, E.; Göktürk, S., Adsorption characteristics of sulfamethoxazole and metronidazole on activated carbon. *Sep. Sci. Technol.* **2010,** *45*, 244-255.
84. Ersan, G.; Apul, O. G.; Perreault, F.; Karanfil, T., Adsorption of organic contaminants by graphene nanosheets: A review. *Water Res.* **2017,** *126*, 385-398.

Table of Contents

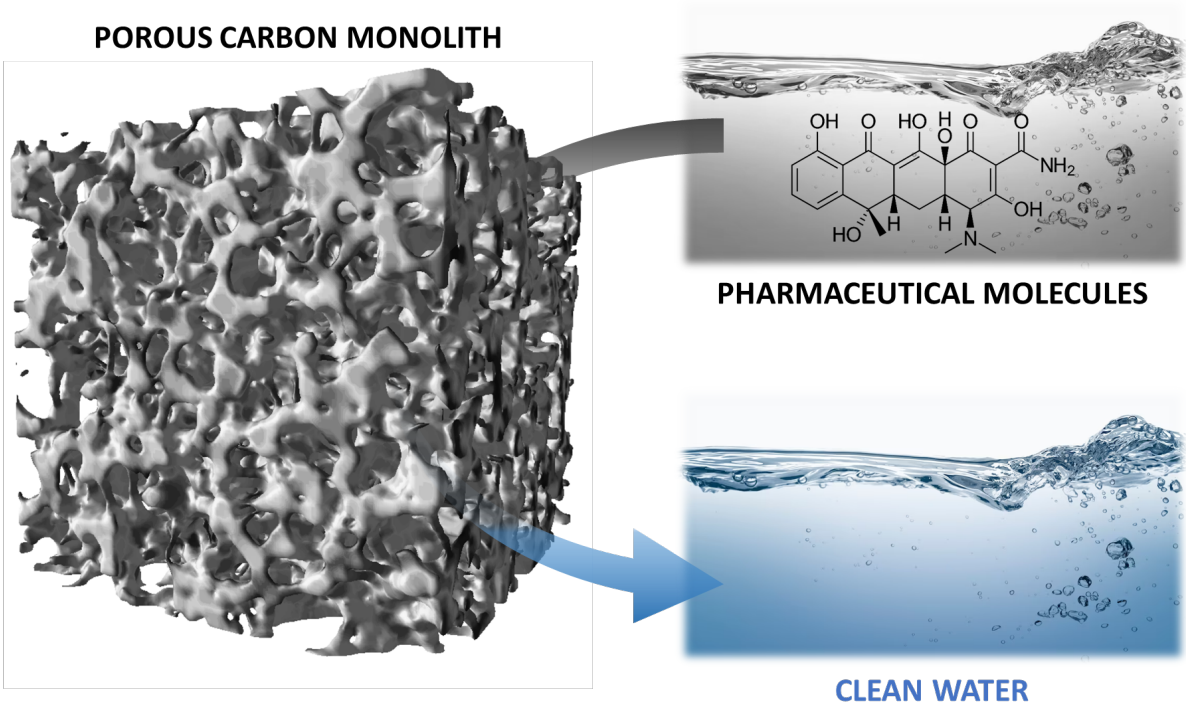

Carbon monoliths with hierarchical porosity could provide a highly efficient solution for the continuous flow purification of real wastewater containing antibiotics.